Condensing and Fluidizing Effects of Ganglioside G_{M1} on Phospholipid Films

Shelli L. Frey,* Eva Y. Chi,* Cristóbal Arratia,† Jaroslaw Majewski,‡ Kristian Kjaer,§¶ and Ka Yee C. Lee*

*Department of Chemistry, Institute for Biophysical Dynamics and James Franck Institute, The University of Chicago, Chicago, Illinois 60637 USA; †Department of Physics, Faculty of Physical and Mathematical Sciences, University of Chile, Santiago, Chile; ‡Manuel Lujan Neutron Scattering Center, Los Alamos National Laboratory, Los Alamos, New Mexico, 87545 USA; §Max-Planck Institute of Colloids and Interfaces, Potsdam, Germany; and ¶Niels Bohr Institute, University of Copenhagen, Copenhagen, Denmark

ABSTRACT Mixed monolayers of the ganglioside G_{M1} and the lipid dipalmitoylphosphatidlycholine (DPPC) at air-water and solid-air interfaces were investigated using various biophysical techniques to ascertain the location and phase behavior of the ganglioside molecules in a mixed membrane. The effects induced by G_{M1} on the mean molecular area of the binary mixtures and the phase behavior of DPPC were followed for G_{M1} concentrations ranging from 5 to 70 mol %. Surface pressure isotherms and fluorescence microscopy imaging of domain formation indicate that at low concentrations of G_{M1} ($<$25 mol %), the monolayer becomes continually more condensed than DPPC upon further addition of ganglioside. At higher G_{M1} concentrations ($>$25 mol %), the mixed monolayer becomes more expanded or fluid-like. After deposition onto a solid substrate, atomic force microscopy imaging of these lipid monolayers showed that G_{M1} and DPPC pack cooperatively in the condensed phase domain to form geometrically packed complexes that are more ordered than either individual component as evidenced by a more extended total height of the complex arising from a well-packed hydrocarbon tail region. Grazing incidence x-ray diffraction on the DPPC/G_{M1} binary mixture provides evidence that ordering can emerge when two otherwise fluid components are mixed together. The addition of G_{M1} to DPPC gives rise to a unit cell that differs from that of a pure DPPC monolayer. To determine the region of the G_{M1} molecule that interacts with the DPPC molecule and causes condensation and subsequent expansion of the monolayer, surface pressure isotherms were obtained with molecules modeling the backbone or headgroup portions of the G_{M1} molecule. The observed concentration-dependent condensing and fluidizing effects are specific to the rigid, sugar headgroup portion of the G_{M1} molecule.

INTRODUCTION

Glycolipids, or lipid molecules containing sugar groups, are present in most animal cell plasma membranes and are thought to regulate various physiological events at the cell surface. The most complex form of glycolipids are gangliosides, which contain one or more negatively charged sialic acid groups. Gangliosides are thought to play roles in a number of cellular functions, including cell recognition and adhesion (1–3), signal transduction (3), and cell growth regulation (4). Although a minor component in most cells, they constitute 5–10% of the total lipid mass in nerve cells (5), and because they reside primarily on the outer leaflet of the cell membrane, the external surfaces of certain cells contain 10–20 mol % ganglioside. One of the most commonly studied gangliosides is G_{M1}, a member of the glycosphingolipid family that contains four neutral sugar groups and one sialic acid residue (Fig. 1). The chemical and structural properties of G_{M1} and other glycolipids have been reviewed extensively (6).

Despite the abundance of glycolipids in the cell, little is known about the lateral structural organization of glycolipids in the outer leaflet of the biological membrane. Characterization of the two-dimensional organization of biological membranes is an important issue that remains to be resolved to understand the structure-function relationships of its components. The raft hypothesis proposes that naturally occurring lipids such as sphingomyelin, glycolipids, cholesterol, and perhaps saturated phospholipids specifically aggregate in the plane of the membrane, driven primarily by lipid-lipid interactions (7). Although the presence and biological role of lipid rafts, or ordered microdomains, in cell surface membranes is still under debate, they are postulated to play important roles in membrane transport and signal transduction (7,8). The current challenge is to determine how individual lipid molecules interact with and affect each other as well as transmembrane proteins to understand the principles behind the structure and dynamics of cell membranes.

Because lipid rafts are implicated to be enriched in gangliosides, as are calveolae, and 30–50 nm invaginations are responsible for endocytosis in plasma membranes, understanding the role of ganglioside molecules in an ordered domain is important. Ganglioside G_{M1} is a surfactant molecule with a bulky, sugar headgroup that cannot form pure bilayer vesicles due to its molecular geometry; in monolayers formed at the air-water interface, surface pressure versus molecular area isotherms indicate that G_{M1} is completely fluid at all surface pressures (9). When combined in specific ternary and quaternary ''lipid raft'' type mixtures, G_{M1} resides in liquid ordered domains (10). In imaging of giant unilamellar vesicles, a low concentration of G_{M1} is a commonly used liquid

Submitted August 17, 2007, and accepted for publication October 26, 2007.

Address reprint requests to Ka Yee C. Lee, E-mail: kayeelee@uchicago.edu.

Editor: Thomas J. McIntosh.

0006-3495/08/04/3047/18 $2.00

doi: 10.1529/biophysj.107.119990

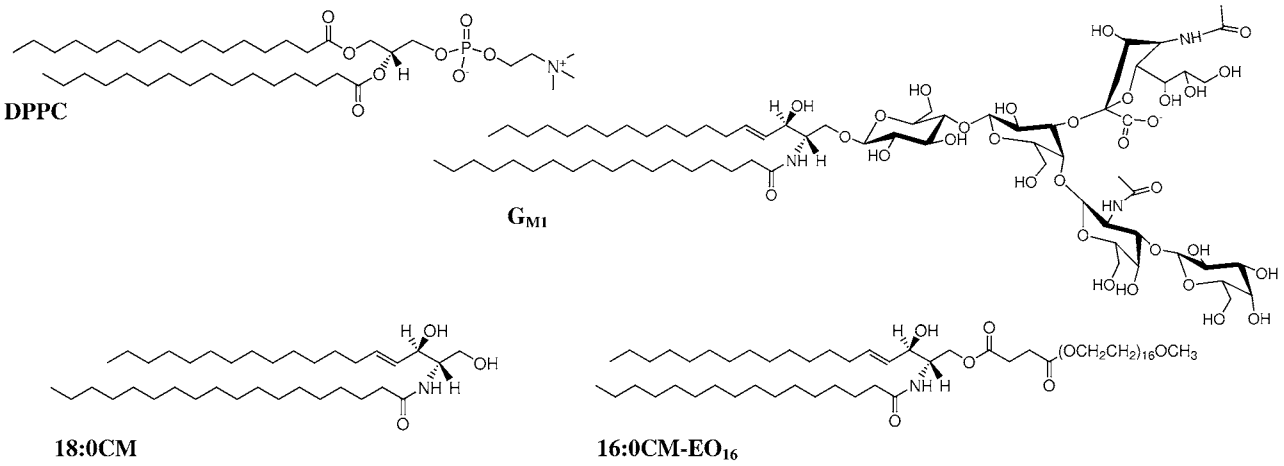

FIGURE 1 Structure of the zwitterionic lipid DPPC, the ganglioside G_{M1}, the ceramide 18:0CM, and the modified ceramide 16:0CM-EO_{16}.

ordered phase, or raft, marker when fluorescently labeled cholera toxin is added to the system and binds to the gangliosides (11). Therefore, certain specific intermolecular interactions must occur between gangliosides and neighboring phospholipids to cause the ''fluid'' molecule to preferentially reside in ordered domains.

Within model membrane systems, conclusions about the lateral organization of G_{M1} and its interactions with neighboring phospholipids have been inconsistent, depending on technique and the chosen model system. High-resolution surface-sensitive techniques such as atomic force microscopy (AFM) have been used to probe the formation of localized submicron-sized domains in phosphatidylcholine (PC) monolayers with low concentrations of G_{M1} deposited on solid supports (12–14). In these studies, G_{M1} was heterogeneously distributed in the layer with clusters of G_{M1}-rich domains found in the gel phase PC domains. However, the lateral organization of the ganglioside within the membrane as well as the driving forces that cause this organization within the phospholipid-G_{M1} mixtures are not well established. Although electron spin resonance (ESR) and freeze fraction studies have implied that G_{M1} preferentially localized with gel state lipids due to hydrogen bonding of the carbohydrate headgroups (15,16), differential scanning calorimetry (17,18) and freeze-etch electron microscopy measurements (18) are more consistent with a random distribution of gangliosides. For example, differential scanning calorimetry studies of PC membranes with low concentration of ganglioside indicate that phase separation of the components does not occur, suggesting that ganglioside is completely miscible with PC (17). In contrast, Delmelle et al. used ESR and spin-labeled gangliosides to conclude that G_{M1} is randomly distributed in the liquid crystalline state and clustered in the gel state (19).

Therefore, the question remains as to what happens to the G_{M1} molecule when placed in a lipid raft-type mixture that allows it to preside in a more condensed or ordered phase than when it is in its pure form. The main motivation for this work was to better understand the influence of G_{M1} on the surrounding lipids and vice versa, by characterizing the physical behavior of a simple model system of zwitterionic lipid dipalmitoylphosphatidlycholine (DPPC) and ganglioside G_{M1} monolayers. Lipid monolayers were used to model the outer leaflet of a cellular bilayer membrane. Additionally, the use of monolayers enabled us to test the full range of G_{M1} concentrations, from 0 to 100%, which can amplify any weak ganglioside-lipid interactions that may be found at biologically relevant G_{M1} concentrations. Although mixtures with $>$20 mol % G_{M1} will not be found within a cell membrane, higher amounts of ganglioside allowed us to test and establish a molecular model of how DPPC interacts with G_{M1} at lower, more realistic concentrations.

The behavior of the phospholipid-G_{M1} mixtures of various mole ratios was initially analyzed in terms of surface pressure versus molecular area isotherms and the resultant mean molecular areas at specific surface pressures. A curious result followed that at low concentrations of G_{M1} ($<$25 mol %), the mixed monolayer was continually more condensed compared to the pure individual constituent monolayers of DPPC and G_{M1} (20). Upon further addition of G_{M1} beyond 25 mol %, the expected expansion due to addition of the bulky, fluid G_{M1} component began to take place. The monolayers were also imaged with fluorescence microscopy (FM) during isothermal compression, and resulting analysis of condensed domain formation and percent surface area coverage supported the conclusion that addition of low concentrations of G_{M1} leads to condensation of the DPPC monolayer followed by fluidization at higher concentrations of ganglioside. Each monolayer mixture was subsequently deposited from the air-water interface onto a solid support, and AFM imaging was performed to study the morphology and phase separation with submicron resolution. Our results demonstrate that at low concentrations, G_{M1} localizes in the condensed domains of DPPC monolayers, preferentially clustering with neighboring DPPC molecules to form a taller DPPC/G_{M1} region

where the molecules pack more tightly and have extended headgroups and hydrocarbon tails. At higher concentrations of G_{M1}, the condensed domains are primarily composed of these G_{M1}-enriched condensed complexes, whereas excess G_{M1} partitions to the fluid phase of the monolayer. Grazing incidence x-ray diffraction, a technique that provides a measure of lateral organization within the monolayer, indicates that the addition of a low concentration of the fluid component, G_{M1}, to a fluid monolayer of DPPC results in a film with ordered domains; registry between the hydrocarbon tails is induced by the presence of GM_1. To determine the structural aspect of the ganglioside molecule that is responsible for this curious condensation effect, parallel isotherm experiments were performed with analog molecules to delineate structural features needed for the observed effect. The results indicate the necessity of a rigid, bulky sugar headgroup for this condensation – fluidization behavior.

MATERIALS AND METHODS

Lipids and subphase

1,2-Dipalmitoylphosphatidylcholine (DPPC), ganglioside G_{M1}, *n*-stearoyl-D-erythro-sphingosine (18:0 ceramide (CM)), and *N*-palmitoyl-sphingosine-1-[succinyl(methoxy(polyethylene glycol)750] (C16 mPEG 750 CM or CM-EO_{16}) (Fig. 1) were obtained in powder form from Avanti Polar Lipids (Alabaster, AL) and used without further purification. The fluorescent probe used for visualization with FM was Texas Red-labeled 1,2-dihexadecanoyl-*sn*-glycerol-3-phosphoethanolamine (TR-DHPE) (Molecular Probes, Eugene, OR). Monolayer spreading solutions were prepared by dissolving in either chloroform (high-performance liquid chromatography grade, Fisher Scientific, Pittsburgh, PA) (e.g., DPPC) or chloroform containing 10% methanol (e.g., binary mixtures of DPPC and G_{M1}) at a concentration of 0.2 mg/ml and adding 0.5 mol % of TR-DHPE. Lipid solutions were stored at −20°C in glass vials. For all Langmuir trough experiments, the subphase was ultra-pure water (resistivity $\geq$ 18 MΩcm) processed by a Milli-Q ultrapurification system (A-10 gradient, Millipore, Bedford, MA).

Instrument setup

Details of the Langmuir trough setup have been discussed previously (21,22). Briefly, the setup consisted of a custom-made Teflon trough equipped with two Teflon barriers whose motions were precisely controlled by a pair of translational stages (UTM100, Newport, Irvine, CA) for symmetric compression or expansion of monolayers at the air-water interface. A stationary Wilhelmy balance (Riegler and Kirstein, Berlin, Germany) is used to measure surface pressure. Subphase temperature was maintained within 0.5°C of the desired temperature with a homebuilt control station composed of thermoelectric units (Marlow Industries, Dallas, TX) joined to a heat sink held at 20°C by a Neslab (Portsmouth, NH) RTE-100 water circulator. A piece of resistively heated coverglass (Delta Technologies, Dallas, TX) was placed over the trough and held at a temperature to suppress evaporative losses, minimize convective currents, and prevent condensation of water on the microscope objective.

The trough assembly was fixed to a custom-built microscope stage to allow simultaneous fluorescence microscopy with a 50× extra-long working distance objective (Nikon Y-FL, Fryer, Huntley, IL). A high-pressure mercury lamp (Osram Sylvania, Danvers, MA) was used for fluorescence excitation and the emitted light was gathered with a dichroic mirror/filter cube (Nikon HYQ Texas Red, Fryer). Images from the fluorescence microscope were collected at a rate of 30 frames/s using a charge-coupled device camera (Stanford Photonics, Palo Alto, CA), and recorded on a Sony digital videocassette with a recorder (Sony, B&H Photo-Video, New York, NY). This assembly permits monolayer morphology to be observed over a large lateral area while isotherm data are obtained. The entire assembly is mounted on a vibration isolation table (Newport, Irvine, CA) and controlled by a custom software interface written using LabView 6.1 (National Instruments, Dallas, TX).

Lateral compression experiments

All experiments were performed at 30°C on pure water. The lipid monolayer was spread by dropwise addition of the spreading solution on the water surface, and the organic solvent was allowed to evaporate for 15 min. The barriers were then compressed with a linear speed of 0.1 mm/s and isotherm measurements in the form of surface pressure (mN/m) versus area per lipid molecule ($Å^2$/molecule) were taken at 1 s intervals until the system reached its compression limit. The isotherm provides information about the phase behavior of the monolayer as a function of lipid-packing density.

Fluorescence microscopy

During the course of all compression experiments, FM images of the surface morphology were recorded on digital videotape. Due to steric hindrance, the fluorescent molecule, TR-DHPE, partitions into the fluid region, rendering it bright and the condensed phase dark, allowing phase information to be extracted (23).

Atomic force microscopy

Higher resolution imaging, i.e., submicron, of the various monolayers transferred from the air-water interface was done with AFM. After isothermal compression at 30°C, lipid monolayers from the Langmuir trough were transferred onto mica substrates by an inverse Langmuir-Schaefer transfer technique similar to that in Lee et al. (24). A freshly cleaved mica substrate was placed in a stainless steel apparatus with a surrounding 2 mm high machined knife edge, and the entire setup placed on the bottom of the trough where it remained submerged in the subphase throughout the compression isotherm. At the desired surface pressure, the subphase was slowly aspirated from the trough to lower the subphase level and the knife edge cut the monolayer as the surface height lowered, preserving monolayer morphology. Drilled holes in the bottom of the steel piece allowed water to exit the chamber completely until the monolayer was deposited on the mica surface. Monolayer morphology before, during, and after transfer was monitored with FM to ensure that the transfer process did not perturb the morphology of the lipid film.

Lipid monolayers transferred to mica substrates were imaged at room temperature using a Multimode Nanoscope IIIA scanning probe microscope (Digital Instruments, Santa Barbara, CA) with a Type J scanner in contact mode in air. Silicon nitride tips NP-S (Veeco Probes, Woodbury, NY) with a nominal spring constant of 0.32 N/m were used; the surface of the tips was decontaminated by ultraviolet-generated ozone before sampling (PSD-UV Surface Decontamination System, Novascan, Ames, IA). Substrates were also imaged in tapping mode in air using silicon tips (nominal spring constant of 42 N/m) and minimal force to check for preservation of morphology after imaging in contact mode. As no disruption was found, all substrates were imaged in contact mode.

X-ray diffraction measurements

All synchrotron x-ray measurements were performed with the liquid surface diffractometer (25–27) at the BW1 (undulator) beam line at HASYLAB, DESY (Hamburg, Germany) with an incident x-ray wavelength of $\lambda \sim 1.30$ Å. A thermostatted Langmuir trough, equipped with a Wilhelmy balance and a barrier for surface pressure control, was mounted on the diffractometer. The

trough was enclosed in a sealed and thermostatted ($T = 30°C$) canister flushed with helium to achieve an oxygen level below 1%; this reduced the scattering background and minimizes oxidative beam damage during x-ray scans. As a further precaution against beam damage, the trough was translated by 0.025 mm horizontally across the x-ray beam, in the direction along the barrier compression at every step of the scan. The dimensions of the incoming x-ray beam footprint on the liquid surface were ~2 mm × 50 mm.

X-ray scattering theory and the liquid diffractometer used here have been described previously (26,28,29). Grazing incidence x-ray diffraction (GIXD) was carried out to obtain lateral ordering information of the samples. The scattered intensity is measured by scanning over a range of horizontal scattering vectors $Q_{\mathbf{xy}} \sim (4\pi/\lambda)\sin(2\theta_{xy}/2)$, where $2\theta_{xy}$ is the angle between the incident and diffracted beam projected on the liquid surface. The GIXD intensity resulting from a powder of two-dimensional (2D) crystallites can be represented as Bragg peaks, resolved in the Q_{xy} direction, by integrating the scattered intensity over all the channels of the position-sensitive detector, perpendicular to the interface defined as the Q_z direction. The angular positions of the Bragg peaks determine the d-spacings, $d = 2\pi/Q_{xy}$ (where the Q_{xy} is the position of the maximum of the Bragg peak) for the 2D lattice. From the line widths of the peaks, it is possible to determine the 2D crystalline coherence length L_{xy_hk}, the average distance in the direction of the reciprocal lattice vector Q_{xy_hk} over which the ordering extends.

RESULTS AND ANALYSIS

DPPC/G_{M1} mixed monolayers

Isotherms of DPPC/G_{M1} monolayers

Surface pressure versus molecular area isotherms was measured for DPPC, G_{M1}, and binary DPPC/G_{M1} monolayers at the air-water interface at 30°C while concurrently imaging with fluorescence microscopy. Fig. 2 shows the overlay of the resulting isotherms. The pure DPPC isotherms are in agreement with published data (30,31), and the phase transitions have been discussed extensively elsewhere (32,33). DPPC goes through the expected gas (G)/liquid expanded (LE) coexistence to lift off in LE phase at 95 Å^2/molecule, then a coexistence plateau where condensed (C) domains start to form at ~20 mN/m, followed by a rapid rise in pressure until the collapse of the monolayer. These phase changes can be correlated with the FM images taken concurrently. The isotherm for pure G_{M1} shows that it is expanded in comparison to that of DPPC as G_{M1} lifts off at a higher area of ~140 Å^2/mol, in agreement with published data (9). According to both isotherm and FM images, G_{M1} remains in the LE phase up to collapse. The fluidity is due to the molecular geometry of G_{M1} with a large headgroup stemming from the steric repulsion of the four sugar groups coupled with electrostatic repulsion of the negatively charged sialic acid (Fig. 1), which prevents the molecules from tightly packing. Regardless of the amount of compression, the large headgroups would not allow the narrower hydrocarbon tails to align to form crystalline domains at this temperature.

In the case of binary mixtures of the individual components, one can see that at low concentrations of G_{M1} (up to 20 mol %), the isotherms shift to the left of pure DPPC at liftoff, suggesting that the addition of the G_{M1} molecule is having a condensing effect. Our results are counterintuitive because

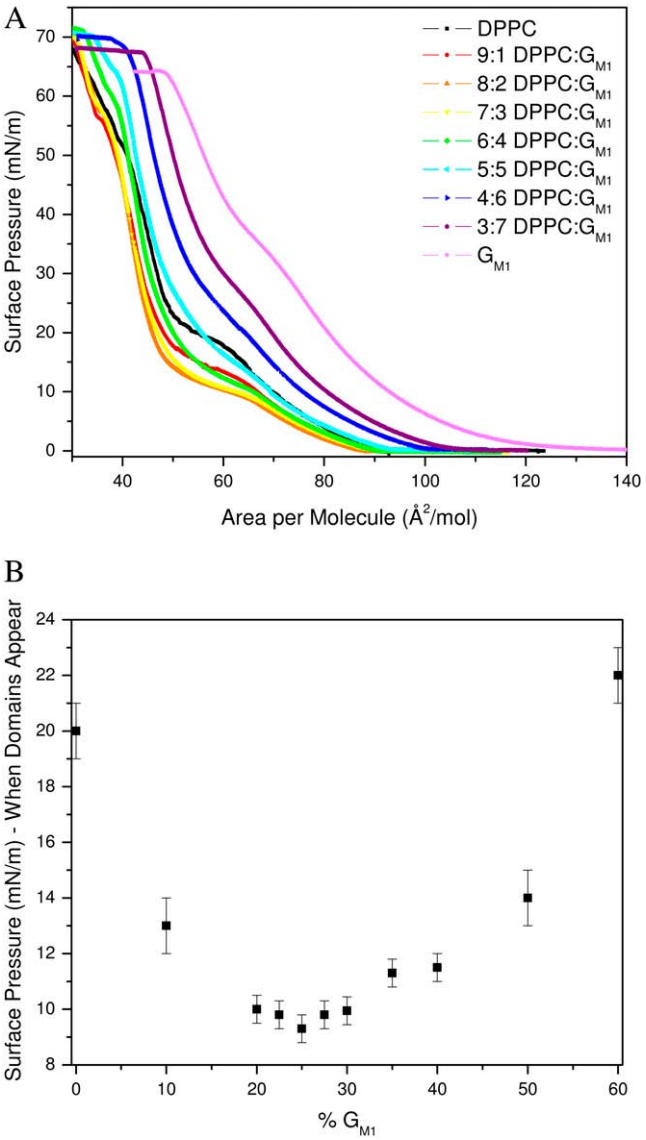

FIGURE 2 (*A*) Monolayer compression isotherms of pure DPPC, pure G_{M1}, and binary mixtures of 9:1, 8:2, 7:3, 6:4, 5:5, 4:6, and 3:7 mol ratio DPPC/G_{M1} at 30°C (*B*) Surface pressure at which condensed (C) domains appear in monolayers composed of DPPC and G_{M1}, plotted as a function of G_{M1} concentration. Domains were visualized using fluorescence microscopy with the TR-DHPE probe partitioning into the more fluid phase.

the ganglioside is fluid by itself, and one would expect it to fluidize the DPPC monolayer, as in the case of adding an unsaturated, fluid lipid to DPPC (34). Further addition of ganglioside (>30% G_{M1}) shifts the liftoff to a higher average area per molecule. In terms of mean area per molecule, the pure DPPC isotherm is most similar to that of a 5:5 DPPC/G_{M1} mixture; regardless of the addition of a molecule with a bulky, sterically hindered headgroup, the average area per molecule of these two systems at liftoff is equivalent.

A correlation in the surface pressure at which the condensed C domains form as a function of the DPPC/G_{M1} ratio is established by the surface pressure of the plateau in the

isotherm in Fig. 2 *B*. The strong dependence on the ratio of components of the binary mixture can be seen plotted in Fig. 2 *B*, where there is an apparent minimum at ~75:25 (or 3:1) DPPC/G_{M1}; subsequent addition of G_{M1} leads to a higher surface pressure at which condensed domains nucleate. Because the determination of surface pressure at which domains form has inherent experimental error, the ''turnaround'' region is relatively flat from 8:2 to 7:3 DPPC/G_{M1}. This region of minimum surface pressure indicates that this binary mixture can pack in a most compact fashion with a stoichiometry of ~3 DPPC molecules to 1 ganglioside, suggestive of a preferred type of molecular packing due to geometrical constraints of each molecule, which we will now refer to as geometric complex formation.

To determine how the individual components of DPPC and G_{M1} are interacting with one another in the mixture, one pertinent parameter is the evolution of mean molecular areas with the monolayer composition at a given surface pressure (35). Fig. 3 *A* shows the plot of the experimental mean molecular area at 10, 20, and 30 mN/m versus the percentage of G_{M1} in the DPPC/G_{M1} monolayer. This so-called ''additivity'' plot can indicate possible deviations from ideal mixing. At each surface pressure, the straight line represents ''ideal mixtures'' with the theoretical area, A_{mix}, given by the additivity equation

$$A_{mix} = X_{GM1}A_{GM1} + A_{DPPC}(1 - X_{GM1}), \quad (1)$$

where X_{GM1} is the molar fraction of G_{M1}, and A_{GM1} and A_{DPPC} are the mean molecular areas of G_{M1} and DPPC, respectively, at the corresponding surface pressure, estimated from isotherms of their respective pure monolayers. If the additivity plot follows the ideal mixing line, this indicates a miscible or completely homogenous film where the components mix but do not interact. It can also indicate that the two components are immiscible, essentially patches of one component in a monolayer of the other. Deviations from the ideal mixing line are evidence of miscibility with molecular interactions between the components.

The average molecular areas in Fig. 3 *A* clearly show that the binary mixtures of DPPC and G_{M1} are at a smaller molecular area or more condensed compared to the ideal system. This indicates specific condensing molecular interactions between the components upon mixing. The binary mixture with the furthest deviation from ideal occurs between 20 mol % and 30 mol % of G_{M1}. If one assumes that the most condensed monolayer is a product of DPPC forming a geometric complex or tight packing with G_{M1} in an ~3:1 ratio, any further addition of G_{M1} to the system would result in G_{M1} in excess, and therefore phase separate out of the system. Fig. 3 *B* shows an additivity plot where the two components in the binary mixture are defined as 7:3 DPPC/G_{M1} and G_{M1}, and it can be seen that in this estimation, the components mix ideally—that is, the additivity plot follows the straight ideal mixing line. To ascertain the stoichiometry of the condensed geometric complex, additivity lines were plotted assuming

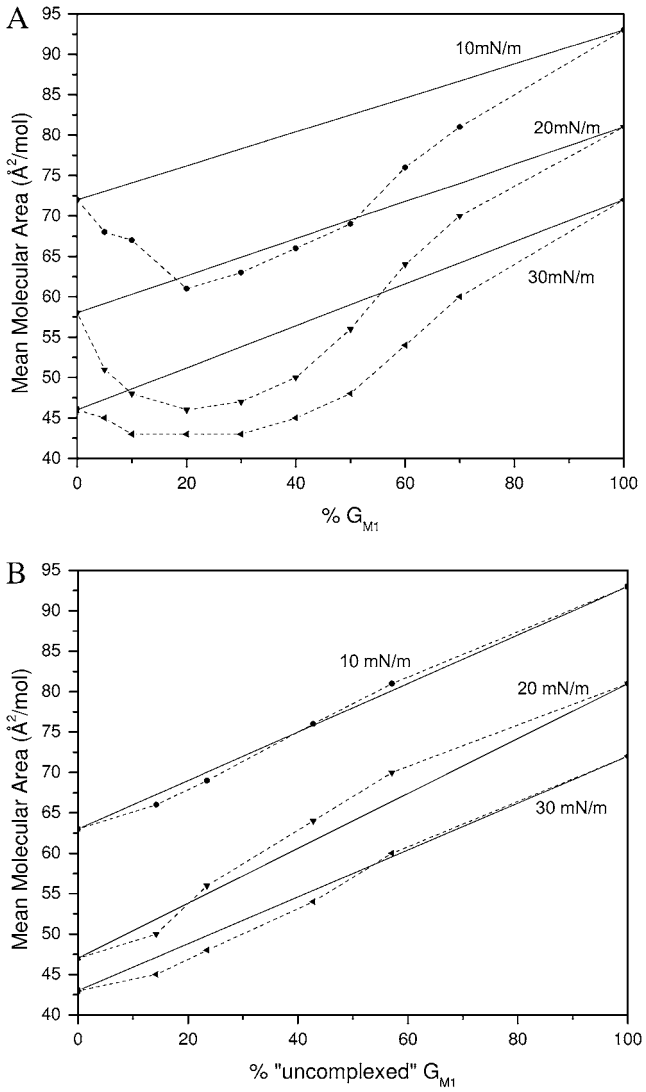

FIGURE 3 Mean area per molecule in mixed monolayers of DPPC and G_{M1} at surface pressures of 10, 20, and 30 mN/m. The solid lines represent values calculated by the additivity rule and correspond to ideal mixtures. Dashed lines are added to guide the eye. (*A*) Mean area per molecule plotted as a function of the percentage of G_{M1} in the monolayer. (*B*) Mean area per molecule assuming that 7:3 DPPC/G_{M1} and G_{M1} are the ''pure'' components plotted as a function of ''uncomplexed'' G_{M1}. See text for details.

each of the intermediate concentrations from 8:2 to 7:3 was pure, and the 7:3 case followed the ideal mixing curve best. To determine the type of ideal mixing (miscible without interaction versus completely immiscible) of the 7:3 DPPC/G_{M1} and excess G_{M1} system, one can use the surface phase rule developed by Crisp, defined by Eq. 2 for a mixed monolayer at constant temperature and external pressure:

$$F = C^B + C^S - P^B - q + 1, \quad (2)$$

where F is the number of degrees of freedom, $C^B = 2$ the number of components in bulk, $C^S = 2$ the number of components confined to the surface, $P^B = 3$ the number of bulk

phases, and q is the number of surface phases in equilibrium (35). Use of the rule indicates that in the case of a miscible monolayer where $q = 1$, there is one degree of freedom; therefore, collapse pressure will vary with composition. In an immiscible monolayer, $q = 2$ or $F = 0$, which indicates collapse will occur at a fixed pressure corresponding to the component with lower equilibrium spreading pressure. Based on nonconstant collapse pressures as a function of ganglioside concentration as seen in Fig. 2 *A*, it is clear that the components, a 7:3 DPPC/G_{M1} geometric complex and subsequent excess G_{M1}, are miscible and noninteracting.

TABLE 1 Surface area coverage of condensed domains as a function of lipid monolayer composition

Lipid composition	Domain surface area (% of total field)
DPPC	11
9:1 DPPC/G_{M1}	66
8:2 DPPC/G_{M1}	76
75:25 DPPC/G_{M1}	78
7:3 DPPC/G_{M1}	65
6:4 DPPC/G_{M1}	38
5:5 DPPC/G_{M1}	18
4:6 DPPC/G_{M1}	0

Fluorescence microscopy images of DPPC/G_{M1} monolayers

Surface pressure measurements give information about phase behavior averaged over the entire monolayer surface, and should be complemented by direct observation of the monolayer morphology. Fluorescence microscopy is a means to visually determine the phase behavior within a monolayer. A 0.5 mol percentage of head-labeled lipid dye, TR-DHPE, is added to each monolayer. The bulky headgroup prefers the LE region due to steric effects (23); therefore, C domains are dark and the LE or disordered phase is bright. Fig. 4 shows a series of DPPC/G_{M1} monolayer FM micrographs at 20 mN/m. For each image, a light/dark threshold was set and the area percent of dark phase was found as shown in Table 1. A small addition of ganglioside has a remarkable effect on the morphology of the condensed DPPC domains, causing them to be larger and adopt a more ''flower-like'' shape. The total area percentage of condensed phase is highest for the 75:25 DPPC/G_{M1} mixture, which correlates well with the monolayer being most condensed near this ratio. On either side of this value, there is a larger amount of LE phase until a G_{M1} concentration higher than 4:6 DPPC/G_{M1}, at which point the monolayer is in a homogenous bright phase, given the optical resolution of the FM setup, up to its collapse pressure. The relative sizes of the C domains echo this condensation behavior as monolayers with the highest area percent of dark phase also contain the largest C domains on the order of 20 μm in diameter.

Atomic force microscopy of DPPC/G_{M1} monolayers

Although FM allows for imaging surface morphology with the bright phase arising from where the probe molecule resides, it does not provide any detailed molecular level information about the location of individual molecules in each phase. To gain insight on a submicron length scale about the molecular organization within the C domains, AFM was performed on deposited monolayers of pure DPPC and pure G_{M1} as well as binary mixtures of the two at varying mole ratios. Deposition was performed at 30 mN/m from a water subphase onto a mica substrate via an inverse Langmuir-Schaefer technique (24) with this pressure chosen because it is the approximate bilayer equivalent pressure (36). The monolayers were imaged with fluorescence microscopy before, during, and after deposition to ensure that membrane morphology was preserved. Each deposited monolayer sample was imaged using AFM contact mode in air. Samples were also imaged in tapping mode in air, and afforded the same results.

A deposited monolayer of pure DPPC (Fig. 5 *A1*) shows no evidence of a large-scale phase separation typically seen at lower pressures with large, micron-sized condensed domains in coexistence with the surrounded LE phase (13). This is because at ~23 mN/m, there is roughening at the boundary between the LE and C phases, arising from an edge instability caused by differing elastic properties of the two phases (37).

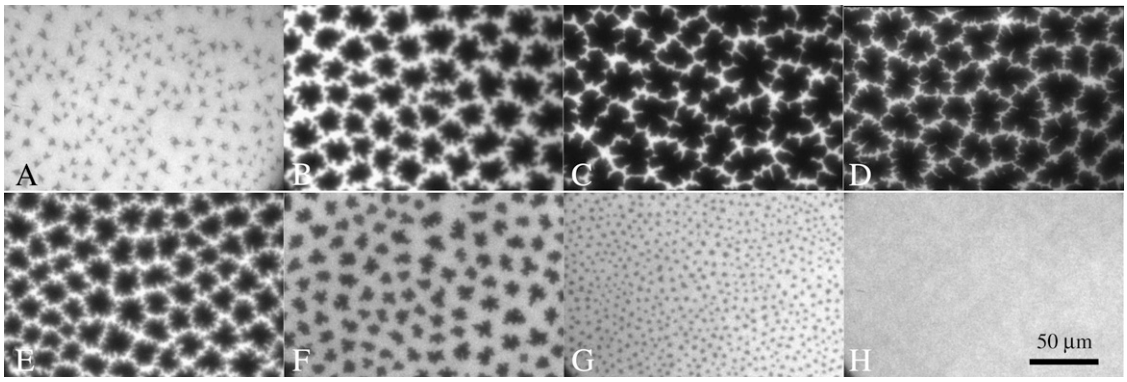

FIGURE 4 Fluorescence images of mixed DPPC/G_{M1} monolayers at a surface pressure of 20 mN/m. (*A*) 100:0. (*B*) 9:1. (*C*) 8:2. (*D*) 75:25. (*E*) 7:3. (*F*) 6:4. (*G*) 5:5. (*H*) 4:6.

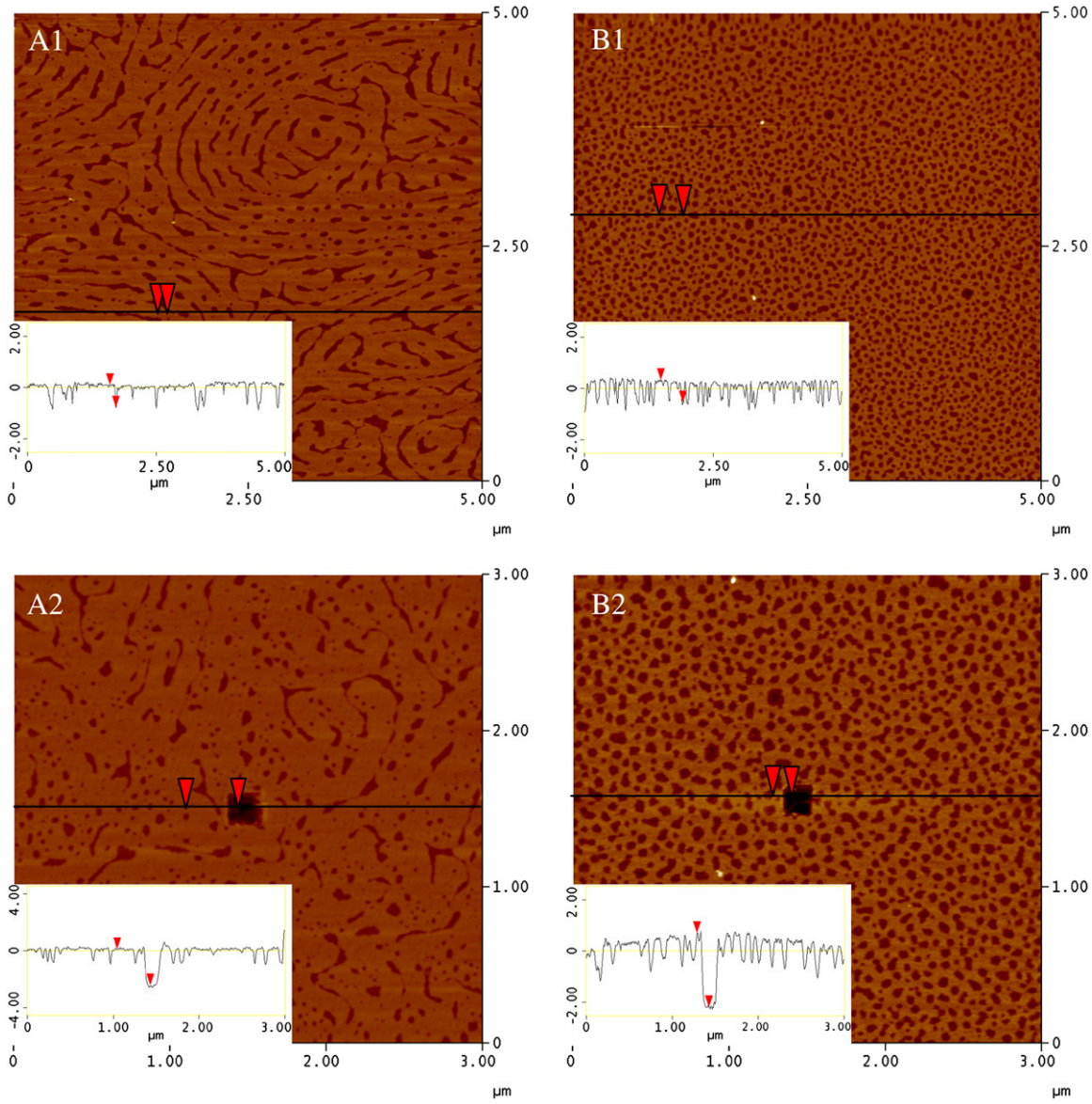

FIGURE 5 AFM topographic images of (*A1* and *A2*) DPPC and (*B1* and *B2*) G_{M1} monolayers transferred at 30 mN/m (*z*-scale 5 nm). Section analysis insets show height differences among the sections (note: lighter in color corresponds to greater height). The dark hole in image (*A2*) DPPC and (*B2*) G_{M1} is a scratched area where the local material was removed by rapidly scanning (20 Hz) a 150 × 150 nm^2 square at high force with the AFM tip. Resulting section analysis insets indicate the total height of the monolayer.

The roughening can be seen with FM as a graying of the interstitial region between domains due to the formation of narrow protrusions beyond the resolution of optical microscopy from the domain boundaries. As the surface pressure increases, the domain boundaries blur and appear to fuse together (data not shown). The resulting deposited monolayer is composed of intricate patterns of C domain stripes interspersed with LE phase. The section analysis inset in Fig. 5 *A1* supports this with a height difference of ~0.8 nm between the two phases, consistent with that reported in the literature (38). A DPPC monolayer deposited at 30 mN/m, but at a lower temperature of 25°C, will have gone through this instability at a lower pressure and give rise to a sheet of condensed domain upon deposition (14). To determine the total height of the deposited DPPC monolayer for comparison with other systems, a 150 nm × 150 nm square area of material was removed with an AFM tip using a high force and scan rate (*dark square* at the center of Fig. 5 *A2*). The section analysis indicates that the total height of the DPPC monolayer in the more condensed and therefore taller phase is ~2.4 nm.

Fig. 5 *B* shows two micrographs for a pure monolayer of G_{M1} deposited at 30 mN/m from a water subphase. Though the corresponding monolayer at the air-water interface in the Langmuir trough shows uniform brightness according to FM measurements, indicating a homogeneous LE phase, the deposited sample is heterogeneous with two heights differing

by ~0.7 nm (see *line scan inset* of Fig. 5 *B1*). Using AFM, it is difficult to determine if this morphology occurs at the air-water interface, but GIXD studies on G_{M1} monolayers indicate a lack of large-scale ordered phase ((39); S. L. Frey, unpublished data), indicating it is likely to be an artifact of the deposition process. Based on the lack of C domain formation as seen via the isotherm or FM, the height difference between the two components may arise from patches of the monolayer being forced to align hydrocarbon tails upon deposition due to the cross-sectional area mismatch between the headgroup and the flexible tail region. In certain cases, deposition of a fluid monolayer onto a solid substrate can result in islands of condensed domains (40). Though it has been suggested that these condensed domains may exist on the water surface but are not detected due to the resolution of fluorescence microscopy, in the case of G_{M1}, it is more likely an artifact of the monolayer transfer process due to the geometry of the molecule. Fig. 5 *B2* is a micrograph of pure G_{M1} where material has been scratched off at the center to reveal a total height of the deposited G_{M1} molecules to be ~2.7 nm. Therefore, a deposited G_{M1} molecule is only 0.3 nm taller in height than the condensed phase of DPPC, even with its bulky sugar headgroup that measures ~1 nm longer than DPPC when fully extended (41). This is likely due to the deposition process affecting the alignment of the bulky sugar group away from a perpendicular orientation, resulting in a reduction in the overall thickness of the film and also causing the formation of domains upon deposition.

The addition of a small amount of ganglioside to a DPPC monolayer to obtain a 9:1 DPPC/G_{M1} mixture has a dramatic effect on the micron-scale morphology. In agreement with the FM image in Fig. 4 *B*, there are well-defined flower-shaped C domains surrounded by a heterogeneous LE phase (Fig. 6 *A*). Upon closer inspection, the C domains are also heterogeneous (Fig. 6 *B*). Within the domain, there is a striped region of ''worm-like'' structures where the bright phase is ~1 nm taller than the surrounding lipid. Toward the edge of the condensed domain region, the striped phase becomes more globular and ends with a ''fence'' built by material (~1 nm taller, noted by the *black arrow* in Fig. 6 *A*) at the edge of the domain. This basic morphology is seen in all of the condensed domains of the deposited 9:1 DPPC/G_{M1} monolayers. Our results demonstrate that G_{M1} preferentially resides in the more ordered condensed phase and that it distributes in clusters. The area of the stripes encompasses ~40% of the C domain, and this area is larger than could be explained by the 10 mol % of G_{M1}. Though this could possibly be due in part to domain broadening stemming from the 10 nm radius of the AFM tip, the increase in area is better explained by DPPC clustering with neighboring G_{M1} molecules and contributing to the taller height region. The total height of the tallest, bright phase is ~3 nm as shown in the section analysis of Fig. 6 *C*, where a small section of material was removed with the AFM tip at high scan rate and force. Note that this is taller than either individual component molecule (DPPC, 2.4 nm; G_{M1}, 2.7 nm) under similar deposition conditions.

Further addition of G_{M1} to form a 7:3 DPPC/G_{M1} deposited monolayer shows changes to the global morphology with roughly circular condensed domains ~15 μm in diameter interspersed in a heterogeneous LE-type phase (Fig. 7 *A1*). By focusing on an area by the highly corrugated domain edge (Fig. 7 *A2*), it can be shown that the condensed domain is primarily composed of a single material, the highest in the micrograph. Scratching a section of material within the condensed domain gave the total height to be ~3.7 nm (*inset* in Fig. 7 *A3*). The heterogeneous LE phase is composed of two heights: one equivalent to the highest component (3.7 nm) in the C domain whereas the other is ~2 nm in height (or ~1.7 nm lower).

A deposited monolayer of 5:5 DPPC/G_{M1} has ~8 μm condensed domains in a monolayer dominated by a heterogeneous (composed of three height components) LE phase (Fig. 7 *B*). Though smaller in diameter, the condensed domains are similar in morphology to those found in the 7:3 DPPC/G_{M1} mixture; the material also has a total single height of 3.7 nm (see *inset* in Fig. 7 *B3*). The LE phase contains materials of three heights. The highest is 3.7 nm, which corresponds to the same height as the material found in the condensed domain. The lowest material is 2.0 nm in height, roughly round in shape and 250 nm in diameter. The intermediate height material is 2.7 nm and constitutes the major morphological difference between the 7:3 and 5:5 DPPC/G_{M1} as well as other binary mixtures with higher ganglioside content. As obvious from our AFM results, the addition of ganglioside G_{M1} to DPPC monolayers has a profound effect on the molecular arrangements and morphology of the layer.

GIXD spectra of DPPC/G_{M1} monolayers

X-ray scattering experiments were performed on DPPC, G_{M1}, and various binary mixtures under the same experimental conditions used for isotherm measurements. GIXD measurements provide in-plane structural information on the ordered, diffracting portion of the monolayer. For lipid monolayers, only the alkyl tails are in-plane ordered and therefore are the source of the diffraction signal (28). At a low surface pressure of 15 mN/m and a temperature of 30°C, neither of the pure components of DPPC and G_{M1} exhibits any Bragg peaks, indicating the lack of any lipid in-plane ordering (Fig. 8 *A*, *top* and *bottom curves*). However, when the two components are mixed in various mole fractions at 15 mN/m, resulting scattering from the monolayer shows Bragg peaks (Fig. 8 *A*). This indicates that DPPC and G_{M1}, though disordered in the pure state, combine and laterally arrange at the surface to form more tightly packed layers with in-plane order in the aliphatic chains. At a low, biologically relevant concentration of G_{M1}, as in the 95:5 DPPC/G_{M1} case, there are two resolvable Bragg peaks (a broad peak with a maximum at $Q_{xy} \sim 1.36$ Å^{-1} and a sharper peak with a maximum at $Q_{xy} \sim 1.475$ Å^{-1} corresponding

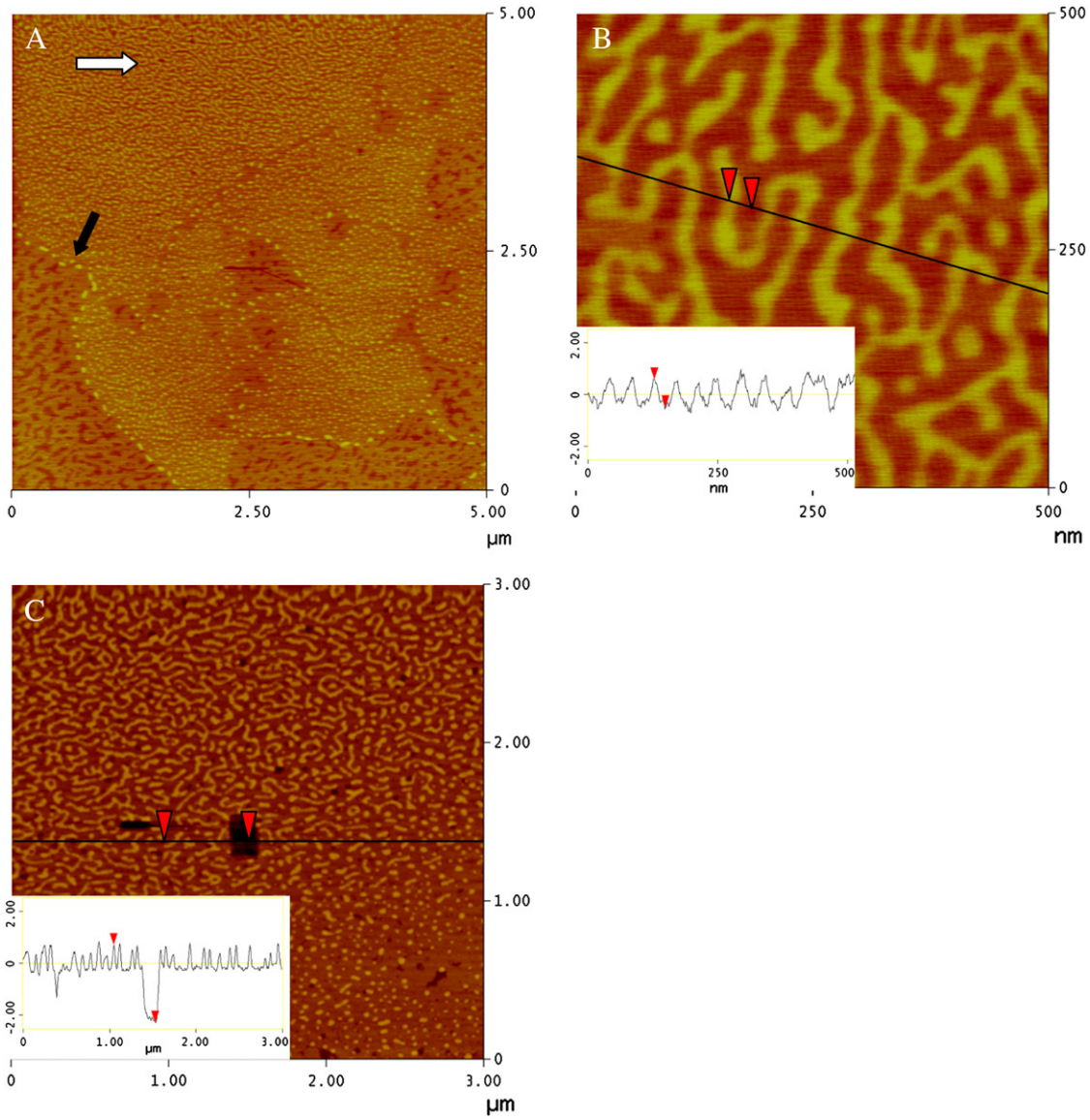

FIGURE 6 AFM topographic images of 9:1 DPPC/G_{M1} monolayers transferred at 30 mN/m (*z*-scale 5 nm). (*A*) Morphology at edge of a condensed domain. Fence of material (~1 nm taller than surroundings) indicated by black arrow. (*B*) Image recorded by zooming into the condensed domain region marked with a white arrow in image *A*. Section analysis inset shows relative height difference between stripes of material. (*C*) Region near edge of condensed domain. The dark hole is a scratched area where the local material was removed by rapidly scanning (20 Hz) a 150 nm square at high force with the AFM tip. Resulting section analysis inset indicates the total height of the monolayer components.

to *d*-spacings of 4.62 Å and 4.26 Å, respectively), indicating a distorted hexagonal unit cell formed by the hydrocarbon tails. For the distorted 2D hexagonal unit cell, the cell unit vectors a_h and b_h have the same length and the angle between them is $\gamma \neq 120°$. Upon further addition of ganglioside, the GIXD spectra become more complex with G_{M1} further condensing the DPPC molecules while also altering the packing parameters. At a higher ganglioside concentration of 75:25 DPPC/G_{M1}, the integrated intensity of the Bragg peaks is highest relative to the other mixtures, indicating the highest area percent of condensed, ordered phase within the x-ray footprint. Additionally, the single peak at $Q_{xy} \sim 1.36$ Å^{-1} seen in the 95:5 mixture becomes two resolvable peaks for 75:25 DPPC/G_{M1}; the system thus gives a total of three Bragg peaks, indicating that the 75:25 DPPC/G_{M1} unit cell becomes oblique. For the oblique 2D hexagonal unit cell, the cell unit vectors a_h and b_h have different lengths and the angle between them is $\gamma \neq 120°$. Two broad Bragg peaks (similar to the 95:5 case) are observed from a 6:4 DPPC/G_{M1} film, but the integrated intensity and therefore the area coverage of condensed domains are low compared to the 75:25 mixture.

To estimate the degree of lateral order induced by G_{M1}, GIXD spectra of pure DPPC and 75:25 DPPC/G_{M1} are shown at 23 and 30 mN/m, and have been offset vertically for clarity (Fig. 8 *B*). At 23 and 30 mN/m and the temperature of 30°C, G_{M1} is completely fluid, exhibiting no Bragg peaks

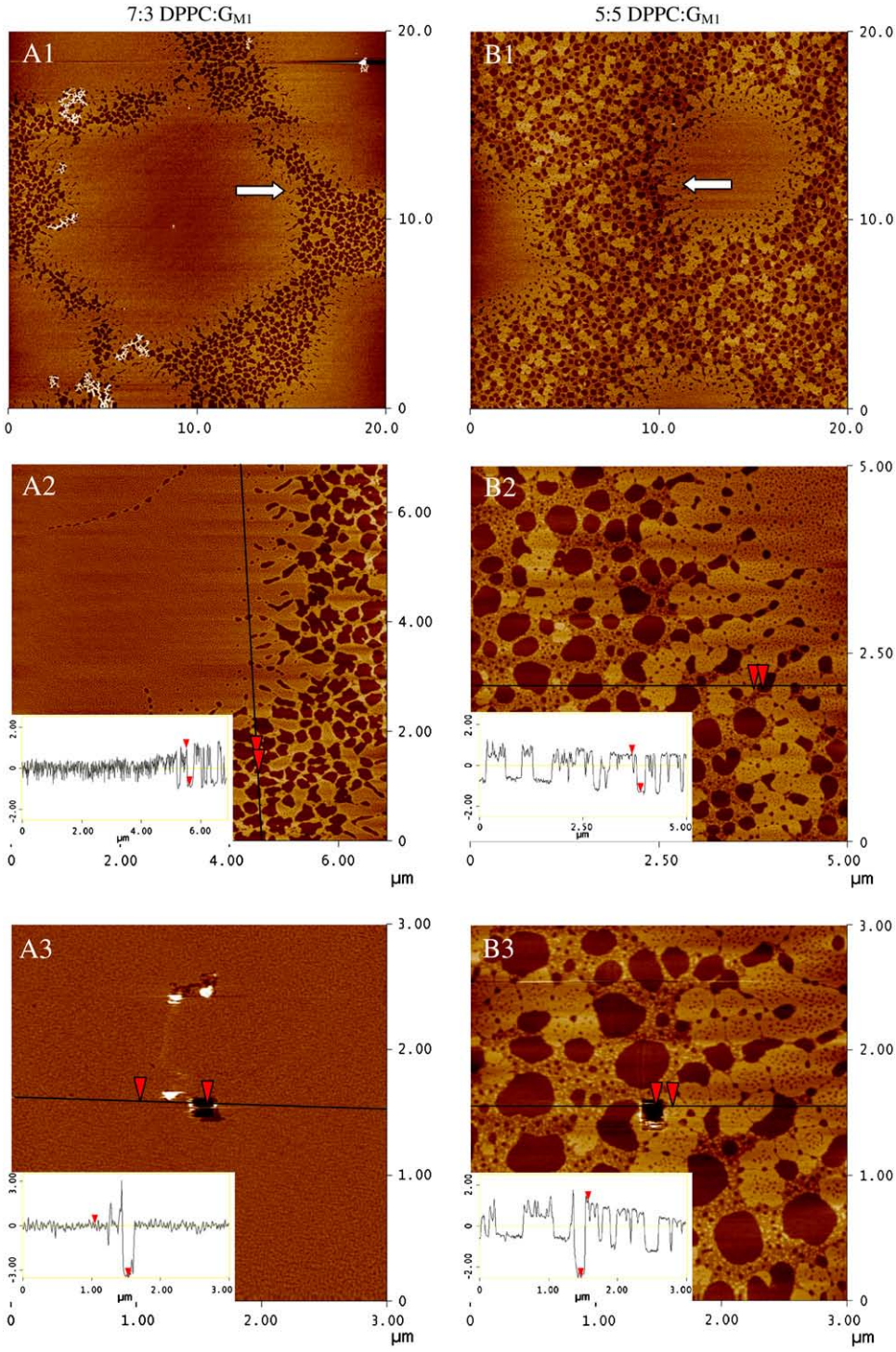

FIGURE 7 AFM topographic images of (*A*) 7:3 and (*B*) 5:5 DPPC/G_{M1} monolayers transferred at 30 mN/m (*z*-scale 5 nm). (*1*) Global morphology. (*2*) Image recorded by zooming into the region at the edge of a condensed domain marked with an arrow in image 1. Section analysis insets show relative height differences among membrane components. (*3*) Region in middle (*A*) or edge (*B*) of condensed domain. The dark hole is a scratched area where the local material was removed by rapidly scanning (20 Hz) a 150 nm square at high force with the AFM tip. Resulting section analysis insets indicate the total height of the monolayer components.

(data not shown). At 23 and 30 mN/m, pure DPPC has two Bragg peaks, indicating a distorted hexagonal unit cell formed by hydrocarbon tails. Addition of G_{M1} to a DPPC monolayer alters the packing of the aliphatic chain unit cell. Unlike the two peaks observed in pure DPPC, the 75:25 DPPC/G_{M1} mixture has three clearly resolved Bragg peaks, arising from a definitive oblique lattice. The corresponding full widths at half-maximum of the Bragg peaks are inversely proportional to the coherence length of the crystalline order according to the Scherrer formula (42). In the case of the binary mixture, the full widths at half-maximum are narrower, compared to DPPC, indicating that addition of G_{M1} causes the ordered domains to be larger and composed of a greater number of molecules. As can be seen from Fig. 8 *B*, the integrated intensity of Bragg peaks of this 75:25 DPPC/ G_{M1} binary mixture is more than twice that of the single component DPPC

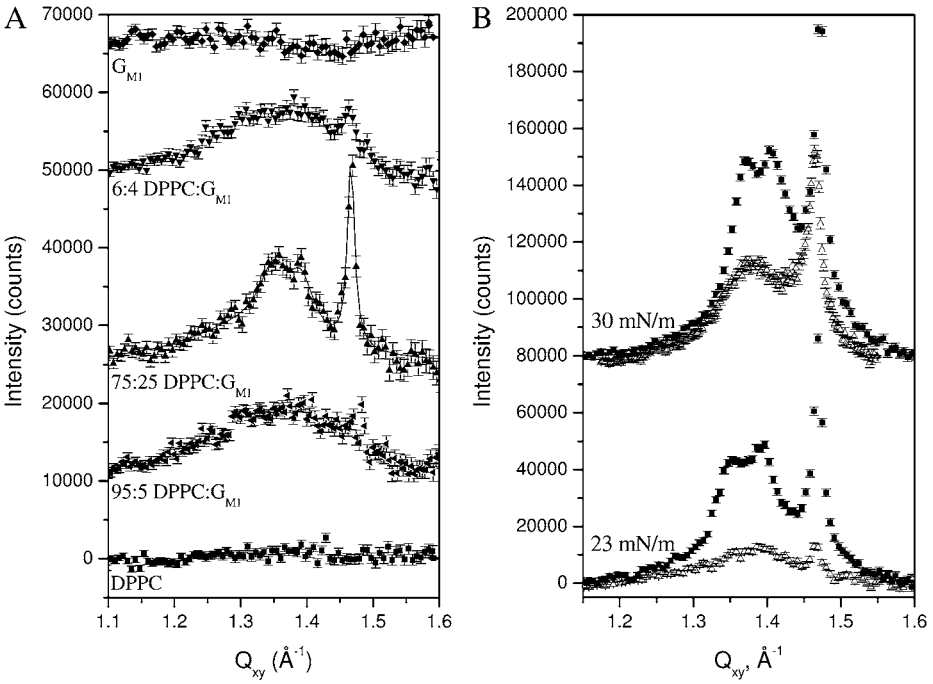

FIGURE 8 Background subtracted GIXD data on a water subphase at 30°C for DPPC, G_{M1}, and various binary mixtures displaying Bragg peaks. (*A*) 100:0 (*squares*), 95:5 (*sideways triangles*), 75:25 (*triangles*), 6:4 (*inverted triangles*), and 0:100 DPPC/G_{M1} (*diamonds*) at 15 mN/m. For clarity, the data have been offset vertically. Note the two pure components have no Bragg peaks, indicating a lack of in-plane order in the tail region. (*B*) Comparison of DPPC (*open triangles*) and 75:25 DPPC/G_{M1} (*squares*) at 23 (*lower panel*) and 30 mN/m (*upper panel*) to show the difference in type and degree of ordering. For clarity, the data at the two pressures have been offset vertically.

monolayer. A detailed analysis of the x-ray diffraction and reflectivity data including the fits that result in a molecular model will be the subject of a separate study.

Modeling G_{M1} structure

In comparison to the structure of a phospholipid, a G_{M1} molecule is unique with a CM backbone, and a relatively rigid, bulky, water-soluble headgroup composed of various sugars and a negatively charged sialic acid. To determine the region of the ganglioside molecule that gives rise to its unique mixing behavior with DPPC in monolayers, the backbone was modeled using CM (Fig. 1), which is essentially G_{M1} without its headgroup. Additionally, the bulky headgroup was modeled with CM-EO_{16} (Fig. 1), a molecule with the same CM backbone as G_{M1} but with a covalently attached polyethylene oxide chain that serves as a bulky but flexible headgroup to model steric interactions. The polymer chain of CM-EO_{16} has a radius of gyration similar to that of the G_{M1} headgroup, but it lacks both the rigidity and the electrostatic interactions (EO is uncharged) of the ganglioside headgroup.

Isotherms of DPPC/CM

Surface pressure versus molecular area isotherms were measured for binary mixtures of DPPC and CM (Fig. 9 *A*) while concurrently imaging with fluorescence microscopy. Pure DPPC behaves as described earlier. At a high area per molecule and surface pressure of 0 mN/m, CM is in a G/C phase coexistence until the isotherm lifts off at ~45 Å^2/molecule, at which point the monolayer is completely condensed and remains so until collapse at 45 mN/m. At 30°C, CM is solid at all appreciable surface pressures whereas G_{M1} is fluid, suggestive of the dominant role of the bulky sugar headgroup in determining the phase behavior of the ganglioside monolayer.

The isotherms for the mixed DPPC/CM films fall between those of the two pure surfactant monolayers, with the addition of CM lowering the mean area per molecule in all cases, such that the higher the mole fraction of CM, the more condensed the film. This is reflected in the FM images of the binary mixtures where C domains exist at a surface pressure of 0 mN/m for all DPPC/CM ratios (data not shown). The surface pressure plateau that occurs in mixtures of low CM concentration ($\leq$25%) does not correlate with the formation of condensed domains, but rather with the edge instability of DPPC caused by differing elastic properties of the two phases (37). The roughening seen with FM is an array of chiral spikes from the condensed domains into the interstitial region until the domains appear to fuse together (data not shown). At higher concentrations of CM, the plateau and edge instability arising from DPPC are absent.

In contrast to the DPPC/G_{M1} mixtures, the isotherms with CM have no turnaround point that would indicate a crossover from condensation to fluidization of the monolayer. Fig. 9 *B* shows the plot of the experimental mean molecular area at 10, 20, and 30 mN/m versus the percentage of CM in the DPPC/CM monolayer with the straight line representing ''ideal mixtures'' as described earlier in Eq. 1. At the lower surface pressures of 10 and 20 mN/m, the average molecular areas indicate that the binary mixtures are at a smaller area per molecule or condensed compared to ideal mixing. At 30 mN/m, however, all DPPC/CM mixtures behave ideally and are shown to be miscible and noninteracting via the Crisp surface phase rule (Eq. 2) (35). Though the additivity plots indicate

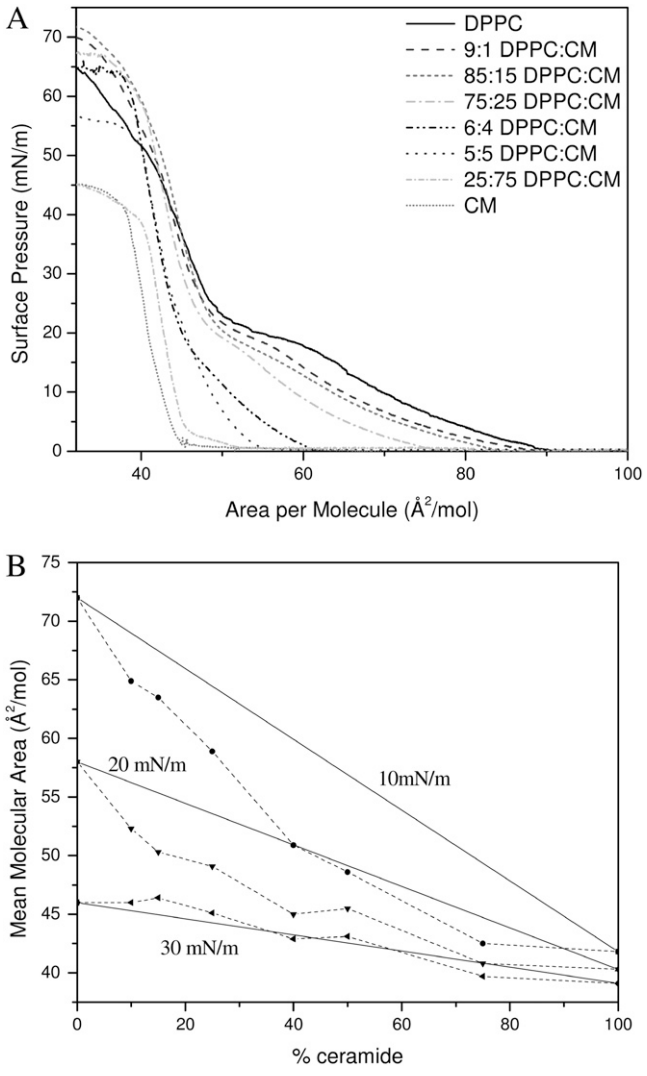

FIGURE 9 (*A*) Monolayer compression isotherms of pure DPPC, pure CM, and binary mixtures of 9:1, 85:15, 75:25, 6:4, 5:5, and 25:75 mol ratio DPPC/CM at 30°C (*B*) Mean area per molecule in mixed monolayers of DPPC and CM at surface pressures of 10, 20, and 30 mN/m plotted as a function of the percentage of CM in the monolayer. The solid lines represent values calculated by the additivity rule and correspond to ideal mixtures. Dashed lines are added to guide the eye.

molecular interactions among the individual components, addition of CM to DPPC is shown to condense the monolayer in all cases. This indicates that for the condensing effect observed in the DPPC/CM system, the role that CM plays is quite different from that of the fluid surfactant, G_{M1} in the DPPC/G_{M1} system. Unlike the binary mixture of DPPC and G_{M1} where the latter is the fluid surfactant, CM is the less fluid component in its binary mixture with DPPC, which serves to better condense a DPPC phospholipid layer.

Isotherms of DPPC/CM-EO$_{16}$

Surface pressure versus molecular area isotherms was measured for binary mixtures of DPPC and CM-EO_{16} at 30°C (Fig. 10 *A*) while concurrently imaging with fluorescence microscopy. An EO_{16} polymer chain has a Flory radius of gyration of ~1 nm in its expanded coil or mushroom configurations ($R_f = aN^{3/5}$, where a is the size of the monomer unit and N is the number of monomers), which is similar to the size of an extended G_{M1} headgroup (39,41). A monolayer of CM-EO_{16} has a liftoff from a G/LE coexistence to LE phase at an area per molecule of ~750 Å^2/molecule. When the PEGylated molecules are at low density at the interface, the 16 subunit polymer chain attached to the CM backbone is surface-active (43), energetically stable at the air-water interface, and contributes to the high surface area of the molecule at liftoff. At high surface pressures ($\Pi > 30$ mN/m), the lateral interactions of the polymer chains are not evident in the pressure isotherm, as isotherms with different amounts of CM- EO_{16} almost all collapse to a single curve in this surface pressure regime. At this point, the polymer is in a brush conformation, with the chains completely submerged in the water subphase. Though a plateau is not readily apparent in the isotherm, FM imaging shows that CM-EO_{16} forms C domains at 13 mN/m that are small and sparse (data not shown).

Fig. 10 *B* shows the surface pressure at which C domains appear for the binary mixtures. This value decreases linearly from that of DPPC (domains form at 21 mN/m) until 40% CM-EO_{16}, above which the C domain formation pressure remains constant at ~13 mN/m. Fig. 10 *C* displays the plot of the experimental mean molecular area at 10, 20, and 30 mN/m versus the percentage of CM-EO_{16} in the DPPC/CM-EO_{16} monolayer with the straight line representing ''ideal mixtures'' as described by Eq. 1. At all surface pressures and mixture ratios, DPPC/CM-EO_{16} follows the additivity line, indicating ideal mixing; the components appear to be miscible as evidenced by the changing morphology of C domains, from fairly DPPC-looking domains at low CM-EO_{16} concentration, to domains with spiky ''petals'' emanating from the center, resembling a poinsettia flower at 6:4 DPPC/CM-EO_{16}, to an even more spiky domain shape at 4:6 DPPC/CM-EO_{16} as observed by FM (data not shown). Due to the compression ratio of the Langmuir trough, monolayers with a high concentration of CM-EO_{16} were spread to a surface area smaller than that of liftoff to allow access to the high pressure regime of the isotherm. Even with this precaution, the collapse pressure could not be reached in some cases. Therefore, analysis of miscibility based on collapse pressure could not be done. Our results indicate that the attachment of a flexible polymer headgroup to a CM backbone does not replicate the phase behavior effect of the ganglioside on DPPC, suggesting that the observed effects with G_{M1} are specific to the rigid sugar groups and sialic acid residue present.

DISCUSSION AND CONCLUSIONS

Data from numerous biophysical assays on DPPC/G_{M1} monolayers have been presented to show how G_{M1} affects lateral ordering and phase behavior in DPPC monolayers.

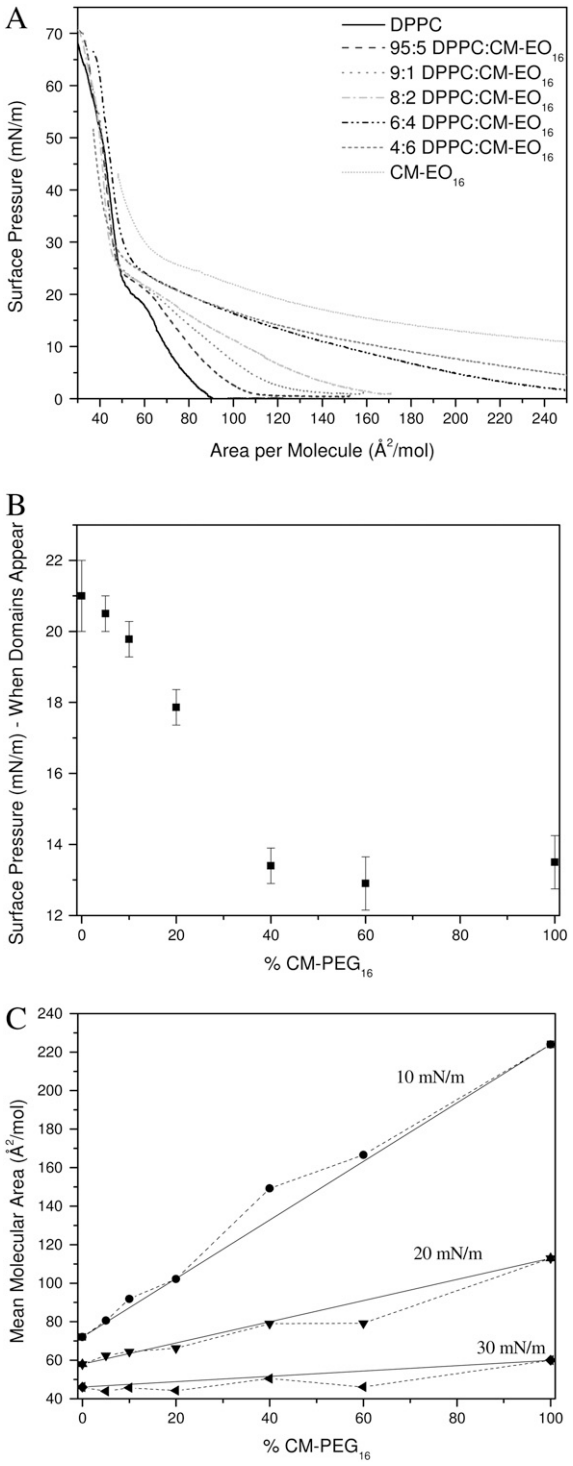

FIGURE 10 (*A*) Monolayer compression isotherms of pure DPPC, pure CM-EO_{16}, and binary mixtures of 95:5, 9:1, 8:2, 6:4, and 4:6 mol ratio DPPC/CM-EO_{16} at 30°C. CM-EO_{16} was deposited at a surface pressure of 5 mN/m. (*B*) Surface pressure at which condensed (C) domains appear in monolayers composed of DPPC and CM-EO_{16}, plotted as a function of CM-EO_{16} concentration. (*C*) Mean area per molecule in mixed monolayers of DPPC and CM-EO_{16} at surface pressures of 10, 20, and 30 mN/m plotted as a function of the percentage of CM-EO_{16} in the monolayer. The solid lines represent values calculated by the additivity rule and correspond to ideal mixtures. Dashed lines are added to guide the eye.

Analysis of isotherms shows that at 30°C, a pure DPPC monolayer has a coexistence plateau at ~20 mN/m where C domains start to form, creating a LE/C coexistence. According to the isotherm and obtained FM images, G_{M1} remains in the LE phase up to collapse. It should be noted that a slight shoulder at 40 mN/m is seen in our isotherm taken at 30°C, and at ~25 mN/m in lower temperature (23°C) isotherms (44), but surface potential measurements have attributed this to changes of electrostatic interactions among the charged headgroups, not formation of ordered domains (44). Additionally, grazing incidence x-ray diffraction of a pure G_{M1} monolayer at 23°C and 40 mN/m provides an in-plane coherence length of 50 ± 10 Å, indicating small crystalline domains only on the order of a few molecules even for a highly compressed G_{M1} monolayer at lower temperatures than used in this work (39). The addition of a low concentration of G_{M1} to a DPPC monolayer results in a binary mixture that is more condensed than either individual component. This is based on the mean area per molecule at liftoff from the G-LE phase and the surface pressure at which condensed domains form. Previous work performed on these systems revealed a similar condensation effect of DPPC monolayers and bilayers on water upon addition of a low concentration of G_{M1} (44–46), but the observed condensing effects differ from the effects reported for DPPC/G_{M1} monolayers run on a buffered subphase where expansion is seen (47). Based on the characterization of the C domains, the pressure they form, and the percent area coverage at a specific surface pressure, the monolayer appears to be most condensed at a ratio of ~75:25 DPPC/G_{M1}. This minimum in area per molecule (or maximum in density) indicates that DPPC and G_{M1} molecules pack most tightly at a set stoichiometry, suggesting the formation of a type of DPPC/G_{M1} complex, packed by geometric constraints, and more condensed than the individual components. If the ratio of three DPPC molecules to one G_{M1} molecule was necessary to form a mixed, well packed complex, the monolayer would actually be composed of a binary mixture of DPPC/G_{M1} geometric complexes and excess DPPC at low concentrations of G_{M1}. On the other hand, at higher G_{M1} concentration, the system would effectively be a binary mixture of DPPC/G_{M1} geometric complexes and excess G_{M1}.

These conclusions are supported by AFM submicron imaging of deposited monolayers used to visualize monolayer morphology and height information of each component to determine the location of molecular species within the layer. The micrographs of the deposited monolayers provide evidence of DPPC forming more tightly packed phases with G_{M1}. The addition of G_{M1} to a DPPC monolayer has marked effects on both the global and local morphology of the film. Previous scanned probe microscopy experiments for DPPC/G_{M1} mixtures with a low (up to 10%) G_{M1} concentration deposited at room temperature display a similar heterogeneous morphology (12–14). In those cases, the C domains were found to be enriched in G_{M1}, but little analysis of the

phenomena was provided. In a mixed monolayer with a low mole percentage of ganglioside (9:1 DPPC/G_{M1}), G_{M1} induces the formation of well-defined 10 μm diameter C domains surrounded by a more fluid, LE phase. In the 9:1 DPPC/G_{M1} monolayer, there is significant heterogeneity within the large condensed domains. There are stripes of material 1 nm taller than the surroundings in the center of the domain, and a ''fence'' of taller material is observed near the edge of the domain. The fluid LE phase was similar in morphology to the LE phase of a DPPC monolayer when deposited at lower pressures before the domain edge instability. Removal of a small area of material with the AFM tip reveals that the bright stripes within the condensed domain of a 9:1 DPPC/G_{M1} monolayer are 3 nm in height, taller than either pure component; DPPC measured 2.4 nm and G_{M1} 2.7 nm under the same deposition conditions.

The high molecular area of G_{M1} found through isotherms and its reduced height compared to that determined by a simple molecular model of 3.7 nm are expected, considering the structure of the G_{M1} headgroup. The head of G_{M1} is a branched, highly hydrated oligosaccharide with a net negative charge (Fig. 1); an electrostatic repulsion is thus expected among the headgroups. This suggests that the packing of the G_{M1} molecules is mainly limited by the headgroup, which maintains a large cross-sectional area at high surface pressure. Even after the headgroups are compressed, there remains ample space for the alkyl tails to assume large tilt angles relative to the surface normal. Infrared reflection absorption spectroscopy experiments have shown that the G_{M1} acyl chains are tilted at the air-water interface by an angle of 37° at 30 mN/m (48). Based on the height and percent area of the striped phase within the condensed domains (both larger than predicted for a 9:1 DPPC/G_{M1} ideally mixed layer), we propose that DPPC is serving as a spacer molecule predominantly between the tail regions of the G_{M1} molecules in the condensed phase as shown in Fig. 11. This allows the bulky sugar headgroups of G_{M1} to interact via hydrogen bonding while the DPPC molecules fill the empty space in the lipid hydrocarbon tail region, reducing molecular tilt and leading to a taller monolayer cross section. Height differences in the AFM micrographs can also be explained by this model, as the condensed domain striped phase is composed of DPPC/G_{M1} geometric complexes in coexistence with condensed DPPC domains whereas the lowest height in the LE region arises from the fluid DPPC. Preliminary analysis of x-ray reflectivity measurements, which provides a measure of electron density distribution perpendicular to the air-water interface, and therefore molecular length, on these mixed systems supports this conclusion of a taller mixed monolayer compared to the pure component heights (S. L. Frey, unpublished data). It has been shown previously that order can be induced in a DPPC monolayer by hexadecanol and palmitic acid, molecules of certain geometry that can act as space-filling molecules and reduce DPPC tail tilt stemming from a head-tail area mismatch, but the mixed monolayer is never more condensed than each pure component (49). In our case, at low surface pressures, both individual components of DPPC and G_{M1} are fluid due to the mismatch of cross-sectional areas of the head and tail region (Fig. 12 *A*). When combined in a binary mixture, the DPPC molecules can fill the void volume between the G_{M1} molecules, causing alignment in the hydrocarbon chain region and therefore decreasing the tail tilt of both species (Fig. 12 *B*). Upon deposition, the DPPC molecules in a well-packed configuration with G_{M1} would contribute to the surface area of the tallest, striped region. It should be noted the molecular configuration should not be viewed as a static one, but rather the headgroup regions of DPPC and G_{M1} can have different possible conformations. The space-filling model shown in Fig. 12 *B* is thus only a first-order approximation to demonstrate how the condensation of the lipid and the decrease of the tilt of the tail group may occur. At low ganglioside concentration, to the left side of the turnaround GM_1 concentration as found in Fig. 2 *B*, or 9:1 DPPC/G_{M1}, the condensed domains are composed of well-packed DPPC/G_{M1} geometric complexes in equilibrium with condensed DPPC, whereas the excess DPPC resides in the LE region.

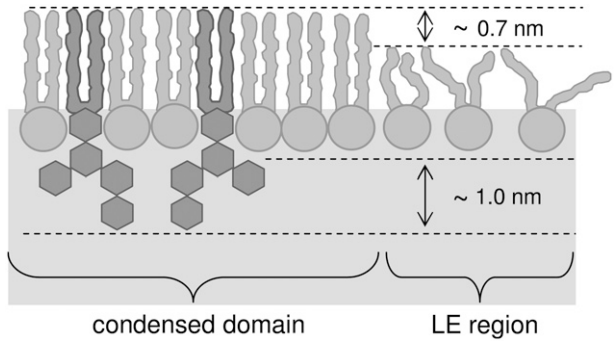

FIGURE 11 Model of DPPC and G_{M1} monolayer at the air-water interface at low G_{M1} concentrations. Regions with DPPC/G_{M1} geometric complexes have a thickness of 3.7 nm. The headgroup of G_{M1} is ~1.0 nm longer than that of DPPC. The height difference between an ordered and a disordered DPPC domain is ~0.7 nm.

Though there are numerous mentions in the literature of the possibility of a hydrogen bonding network among the headgroups of G_{M1}, detailed NMR studies show that when the headgroups are brought into close proximity of one another in micellar form, there is no evidence of intermolecular carbohydrate-carbohydrate interactions (50,51). Each ganglioside has a large shell of associated motion-restricted water (~25–30 water molecules) around each headgroup that could mediate long-range interactions among monomers and not be detected by NMR experiments (52). Conversely, ESR measurements of G_{M1} in phospholipid bilayers indicate that the oligosaccharide headgroup is capable of forming intermolecular hydrogen bonds (15). A Fourier transform infrared attenuated total reflection study provides evidence of intermolecular hydrogen bonding among the amide groups of the sialic acid residues (53). Our results indicate that the driving

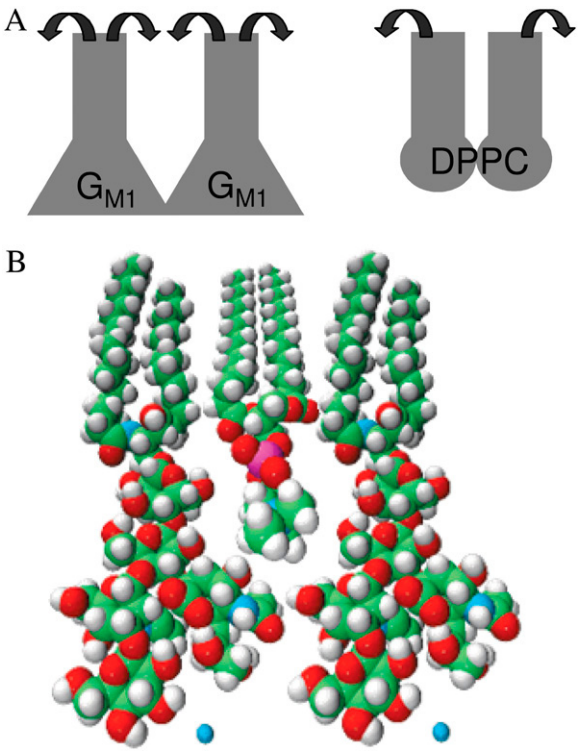

FIGURE 12 (*A*) Representation in terms of geometric shape of each pure component in a monolayer at low surface pressure (~15 mN/m). When the headgroups of each molecule sterically interact, the monolayer remains disordered, or fluid, due to the smaller cross-sectional area of the tail region that allows conformational freedom of the hydrocarbon chains (indicated by the two *arrows* about the tail region). (*B*) Space-filling model of DPPC and G_{M1} in a close-packed or condensed arrangement. Note how the two different molecules, each fluid when in a pure monolayer as shown in *A*, can geometrically pack to reduce mobility in the tail region, causing condensed domains to form.

force to tightly pack the negatively charged headgroups is large enough to induce entropically disfavored ordering of the neighboring molecules. This is not the first study to show condensation behavior in a mixture of a zwitterionic lipid with a charged one. In mixtures of DPPC and phosphatidylinositol-4,5-bis(phosphate) (PIP_2), an acidic phospholipid with a net charge of −3, differential scanning calorimetry and ^{1}H-NMR studies provided evidence of structured regions of DPPC/PIP_2 complexes (54). Numerous studies performed on a binary system of dimyristoyltrimethyl ammonium propane/dimyristoyl phosphatidylcholine (DMTAP/DMPC) indicate that the addition of cationic lipid to a zwitterionic layer causes a condensation of the DMPC molecules neighboring the DMTAP molecules. Through detailed molecular dynamics and theoretical studies, this effect had been attributed to a reorientation of the dipole moment of the PC headgroup leading to electrostatic attraction among the molecules (55–57). A parallel computational analysis of the structural reorganization of the headgroup regions of DPPC and G_{M1} and the subsequent driving force behind condensation is beyond the scope of this work.

Upon further addition of ganglioside resulting in a mixed system on the ganglioside-rich side of the turnaround point in the case of 7:3 and 5:5 DPPC/G_{M1}, the G_{M1} rich stripes in the C domains (as shown in Fig. 6 *B*) grow and merge together to form a primarily single height entity. All excess G_{M1} resides in the LE phase, resulting in fluidization of the monolayer as more G_{M1} is added. Past the turnaround point, all of the DPPC molecules located in the monolayer have formed condensed geometric complexes with G_{M1} in the ideal case, resulting in a well-ordered domain 3.7 nm in height. The complex height found in the G_{M1} rich monolayers (7:3 and 5:5 DPPC/G_{M1}) is taller than that found in the 9:1 DPPC/G_{M1} case, because all of the gangliosides found in the C domains have been optimally surrounded with the necessary number of DPPC molecules, thus further decreasing tail tilt and possibly resulting in the extension of the headgroup. The DPPC spacer is estimated to affect the headgroup region as well, as the 1 nm gain in height compared to pure G_{M1} may not stem only from decreasing the tilt in the tail region; preliminary x-ray reflectivity results support this assumption (S. L. Frey, unpublished data). Based on our tight packing hypothesis, the position of the turnaround point, or alternatively the number of DPPC molecules necessary to pack with G_{M1}, is defined by the relative cross-sectional area of each molecule. Therefore, a ganglioside with a smaller cross-sectional area should require fewer DPPC molecules to form a well-packed condensed phase. Preliminary data from a mixed monolayer system of DPPC and G_{A1}—a ganglioside identical in structure to G_{M1} except the sialic acid residue is removed and therefore has a narrower cross-sectional area—support this argument (S. L. Frey, unpublished data). Alternatively, a phospholipid with a smaller cross-sectional area will require a greater number of lipids to form a geometric complex structure with G_{M1}. A parallel series of experiments with DMPE is in progress to test the effect of the phospholipid headgroup. Since the results from the binary mixtures of DPPC and G_{A1} (an uncharged gangslioside) also show a turnaround behavior with condensation at low concentrations of added ganglioside and expansion of the monolayer at high concentrations, this effect is not primarily governed by the electrostatics of the ganglioside headgroup. This suggests that intramolecular hydrogen bonding among the G_{M1} headgroups and also between DPPC and G_{M1} is a driving force of the condensation effect, whereas the overall respective size of the headgroups dictate the geometry of packing.

To the right side of the turnaround point, all excess molecules are theoretically ganglioside. In the 7:3 DPPC/G_{M1} monolayer, small islands of G_{M1}-rich condensed geometric complex domains (3.7 nm in height) spread into the LE phase, which is primarily composed of a material with the same characteristics and 2 nm height as fluid ganglioside seen in Fig. 5 *B*. At an even higher concentration of G_{M1}, 5:5 DPPC/G_{M1}, the deposited monolayer global morphology looks similar to that of the 7:3 mixture, except for a lower surface area coverage of condensed domains due to there being less total DPPC to form condensed complexes with G_{M1}. There is also an intermediate height (2.7 nm) component in the more

fluid, LE phase that can be attributed, based on its total height, to excess G_{M1} upon deposition.

To obtain a more detailed molecular picture of the interactions of DPPC with the ganglioside G_{M1}, GIXD was performed on pure and mixed monolayers at the air-water interface. At a low surface pressure of 15 mN/m, neither of the individual components exhibited crystalline order as evidenced by a lack of Bragg peaks. Combining the two components at various mole ratios ranging upward from a biologically relevant 5 mol % G_{M1} resulted in a binary mixture that had lateral order, reflected by discernable Bragg peaks. The intensity of the Bragg peaks is indicative of the relative area of crystalline scattering centers in the x-ray beam footprint. Since the point of minimum area (the turnaround point) in the additivity plot (Fig. 2 *B*) defines the stoichiometry at which the monolayer is most condensed and has the highest number of condensed DPPC/G_{M1} geometric complexes, it follows that the highest integrated intensity of the Bragg peaks should be and is seen in the 75:25 DPPC/G_{M1} mixture. At higher surface pressures of 23 and 30 mN/m, a DPPC monolayer exhibits order with a distorted hexagonal unit cell. GIXD experiments performed on a DPPC monolayer compressed to 30 mN/m, but at a lower temperature of 15°C were able to distinguish two peaks within our broad peak at $Q_{xy} = 1.36$ Å^{-1} for a total of three peaks (58). Comparison of the GIXD spectra from the 75:25 DPPC/G_{M1} monolayer clearly shows that inclusion of G_{M1} leads to a higher surface area coverage of condensed phase as evidenced by the increased integrated scattering intensity. Furthermore, the addition of G_{M1} also alters the geometry of the molecular unit cell to a well-discerned oblique lattice stemming from three well-resolved Bragg peaks. These results vary from those of Majewski et al., who used GIXD and x-ray reflectivity to show that inclusion of G_{M1} in a DPPE monolayer did not affect the packing structure of the phospholipid monolayers (39). In those experiments, performed at 23°C, DPPE is below its triple point and already exists in a condensed phase at 45 mN/m where the GIXD spectra were taken. This is in contrast to our experiments, where DPPC can exist as a fluid or a condensed monolayer at 30°C, depending on the surface pressure.

To determine the structural aspects of the ganglioside molecule that contribute to its unique geometric complex formation with DPPC, isotherms were obtained for binary mixtures of DPPC with CM, the backbone of G_{M1}. The CM molecule headgroup region contains both hydrogen bond donors and acceptors as compared to a phospholipid headgroup that has only hydrogen bond donors. Therefore, CM can form a network of hydrogen bonds, causing the pure monolayer to be completely condensed upon liftoff. Although G_{M1} has a CM backbone, the large cross-sectional area of its headgroup as compared to the tail region prevents the molecules from packing into crystalline domains. At low surface pressures, CM serves to condense DPPC at all binary ratios as seen by the isotherms and the formation of condensed domains at a surface pressure of 0 mN/m for all mixtures. Surface pressure measurements on DPPC/CM 3 (a molecule structurally related to CM) monolayers have shown a negative deviation of the average area per molecule from the ideal mixing relation, suggesting an attractive interaction (59). Additivity plots show that at higher surface pressures of 30 mN/m, DPPC and CM mix ideally. This can be explained by the orientation of the individual molecules in their respective pure states. At low pressure, the tail region of a pure DPPC monolayer is tilted as it is in a disordered phase, and the tilt angle reduces upon compression to higher pressures when the acyl chains align. In the absence of a headgroup, CM can be thought of as having an inverted wedge shape, and as already discussed above, CM forms condensed phase upon liftoff. When CM is added to DPPC, CM molecules can intercalate between the once-disordered DPPC tail region, forcing the DPPC tails to condense at low pressures. As the DPPC molecules already are in the condensed phase at high surface pressure with the tilt of the tail group much reduced, the condensing effect of CM observed at low pressures disappears and the binary system appears to mix ideally. Our results echo those of Massey, who used a fluorescence probe technique to show addition of CM to DPPC bilayers resulted in the ordering of the phospholipid acyl chain region with the magnitude of change dependent on the CM composition within the bilayer (60).

To model the effect of steric crowding arising from the headgroup of G_{M1}, a PEGylated CM molecule, CM-EO_{16}, was used. In contrast to G_{M1}, pure monolayers of CM-EO_{16} were not entirely fluid—C domains formed at 13 mN/m. This is because at a high area per molecule, the polymer chain attached to the CM backbone resides at the surface, but at liftoff when the molecules can sense one another, the polymer is pushed into the subphase, giving rise to a pancake-to-mushroom shape transition (61). Upon further lateral compression, the polymer chain attachments are crowded in the subphase and stretch out to avoid neighboring chains; this transition to a brush structure allows the CM portion of the molecule to hydrogen bond and form condensed domains. For a related PEGylated lipid, distearoylphosphatidylethanolamine-EO_{16}, no domain formation or structuring within the monolayer at the air-water interface was observed using fluorescence or Brewster angle microscopy (43), indicating that the CM portion of the molecule is responsible for condensed domains. At concentrations >40 mol % CM-EO_{16}, the surface pressure at which domains form is identical to that of the pure CM-EO_{16}. There are two main opposing forces associated with domain formation in a pure CM-EO_{16} monolayer: the CM backbone that will form hydrogen bonds and therefore promote domain formation, and the polymer chains that will cause steric hindrance among the molecules when they become close and discourage formation of domains. When mixed with DPPC, the CM backbones and the corresponding polymer chains are spread further apart on average. This means that less energy is necessary to separate the polymer chains on the one hand, but on the other hand,

there are also fewer CM backbones to hydrogen bond. At low concentrations of CM-EO_{16}, the PEGylated molecules are spaced far apart from one another, allowing the polymer region to delay the brush transition until the film reaches a higher surface pressure compared to that found in a pure CM-EO_{16} film. As the concentration of CM-EO_{16} is increased, the delay for the brush transition is correspondingly reduced. When a ratio of 6:4 DPPC/CM-EO_{16} is reached, further addition of CM-EO_{16} causes the binary system to form condensed domains at the same surface pressure as that of a pure CM-EO_{16} film, indicating that at this high concentration of PEGylated lipids, the polymer headgroup interaction is similar to that found in a pure CM-EO_{16} monolayer. In contrast to G_{M1}, mixtures of DPPC and CM-EO_{16} mix ideally at all concentrations and pressures, showing that the addition of a flexible, but sterically bulky headgroup to a CM backbone does not approximate the effects of the rigid sugar headgroup of the ganglioside.

Specialized membrane domains composed of phospholipids, glycolipids, and cholesterol, commonly referred to as lipid rafts, are thought to play a role in a diverse range of cellular processes, from membrane trafficking to signaling through specific membrane-protein interactions within the raft microdomain. With all the current interests in lipid raft mixtures, there have been numerous studies about how cholesterol serves as a molecular spacer within the liquid ordered phase of ternary mixtures. Our work here provides evidence that ganglioside G_{M1}, which is also found to be enriched in lipid rafts, alters the phase behavior of neighboring saturated phospholipid molecules, causing a condensation at biologically relevant concentrations as well as altering the phospholipid molecular packing within the condensed domain.

The authors acknowledge beam time at the BW1 beam line at the Deutsches Elektronen-Synchrotron in Hamburg, Germany.

This work was supported by the National Science Foundation (NSF) (MCB-0616249). S.L.F. is grateful for the support of a National Science Foundation Graduate Research Fellowship and an I2CAM travel award (NSF grant DMR 0645461) for the x-ray work. E.Y.C. is grateful for the support by the National Institutes of Health Ruth L. Kirschstein National Research Service Award Individual Fellowship (AG025649) and an I2CAM travel award (NSF grant DMR 0645461) for the x-ray work. The three-month visit of C.A. at Chicago was supported by the Chicago-Chile Exchange Program of the University of Chicago Materials Research Science and Engineering Center of the National Science Foundation (DMR-0213745). J.M. was supported by the Los Alamos National Laboratory under Department of Energy (DOE) contract W7405-ENG-36, the DOE Office of Basic Energy Science. We also received financial support from the DanSync program of the Danish Natural Science Research Council and from the Carlsberg Foundation.

REFERENCES

1. Cheresh, D. A., J. R. Harper, G. Schulz, and R. A. Reisfeld. 1984. Localization of the gangsliosides GD2 and GD3 in adhesion plaques and on the surface or human-melanoma cells. *Proc. Natl. Acad. Sci. USA.* 81:5767–5771.
2. Burns, G. F., C. M. Lucas, G. W. Krissansen, J. A. Werkmeister, D. B. Scanlon, R. J. Simpson, and M. A. Vadas. 1988. Synergism between membrane gangliosides and ARG-GLY-ASP-directed glycoprotein receptors in attachment to matrix proteins by melanoma cells. *J. Cell Biol.* 107:1225–1230.
3. Hakomori, S. 1993. Structure and function of sphingoglycolipids in transmembrane signaling and cell-cell interactions. *Biochem. Soc. Trans.* 21:583–595.
4. Yates, A. J., J. D. Agudelo, and C.-C. Sung. 1992. Glycolipids of a human glioma cell-line bearing receptors for platelet-derived growth-factor (PDGF). *Lipids.* 27:308–310.
5. Derry, D. M., and L. S. Wolfe. 1967. Gangliosides in isolated neurons and glial cells. *Science.* 158:1450–1452.
6. Maggio, B. 1994. The surface behavior of glycoshingolipids in biomembranes: a new frontier of molecular ecology. *Prog. Biophys. Mol. Biol.* 62:55–117.
7. Simons, K., and E. Ikonen. 1997. Functional rafts in cell membranes. *Nature.* 387:569–572.
8. Simons, K., and E. Ikonen. 2000. Cell biology—how cells handle cholesterol. *Science.* 290:1721–1726.
9. Maggio, B., F. A. Cumar, and R. Caputto. 1978. Surface behaviour of gangliosides and related glycospingolipids. *Biochem. J.* 171:559–565.
10. Radhakrishnan, A., T. G. Anderson, and H. M. McConnell. 2000. Condensed complexes, rafts, and the chemical activity of cholesterol in the membrane. *Proc. Natl. Acad. Sci. USA.* 97:12422–12427.
11. Hammond, A. T., F. A. Heberle, T. Baumgart, D. Holowka, B. Baird, and G. W. Feigenson. 2005. Crosslinking a lipid raft component triggers liquid ordered-liquid disordered phase separation in model plasma membranes. *Proc. Natl. Acad. Sci. USA.* 102:6320–6325.
12. Vié, V., N. Van Mau, E. Lesniewska, J. P. Goudonnet, F. Heitz, and C. Le Grimellec. 1998. Distribution of ganglioside G_{M1} between two-component, two-phase phosphatidylcholine monolayers. *Langmuir.* 14:4574–4583.
13. Yuan, C., and L. J. Johnston. 2000. Distribution of ganglioside GM1 in L-α-dipalmitoylphosphatidylcholine/cholesterol monolayers: a model for lipid rafts. *Biophys. J.* 79:2768–2781.
14. Ohta, Y., S. Yokoyama, H. Sakai, and M. Abe. 2004. Membrane properties of mixed ganglioside G_{M1}/phosphatidylcholine monolayers. *Colloids Surf. B.* 33:191–197.
15. Sharom, F. J., and C. W. M. Grant. 1978. Model for ganglioside behavior in cell-membranes. *Biochim. Biophys. Acta.* 507:280–293.
16. Peters, M. W., I. E. Mehlhorn, K. R. Barber, and C. W. M. Grant. 1984. Evidence of a distribution difference between two gangliosides in bilayer membranes. *Biochim. Biophys. Acta.* 778:419–428.
17. Bach, D., I. R. Miller, and B.-A. Sela. 1982. Calorimetric studies on various gangliosides and ganglioside-lipid interactions. *Biochim. Biophys. Acta.* 686:233–239.
18. Thompson, T. E., M. Allietta, R. E. Brown, M. L. Johnson, and T. W. Tillack. 1985. Organization of ganglioside GM1 in phosphatidylcholine bilayers. *Biochim. Biophys. Acta.* 817:229–237.
19. Delmelle, M., S. P. Dufrane, R. Brasseur, and J. M. Ruysschaert. 1980. Clustering of gangliosides in phospholipid bilayers. *FEBS Lett.* 121: 11–14.
20. Chi, E. Y., S. L. Frey, and K. Y. C. Lee. 2007. Gangslioside GM1-mediated amyloid-beta fibrillogenesis and membrane disruption. *Biochemistry.* 46:1913–1924.
21. Gopal, A., and K. Y. C. Lee. 2001. Morphology and collapse transitions in binary phospholipid monolayers. *J. Phys. Chem. B.* 105: 10348–10354.
22. Frey, S. L., and K. Y. C. Lee. 2007. Temperature dependence of poloxamer insertion into and squeeze-out from lipid monolayers. *Langmuir.* 23:2631–2637.
23. Knobler, C. M. 1990. Seeing phenomena in flatland—studies of monolayers by fluorescence microscopy. *Science.* 249:870–874.
24. Lee, K. Y. C., M. M. Lipp, D. Y. Takamoto, J. A. Zasadzinski, and A. J. Waring. 1998. Apparatus for the continuous monitoring of surface morphology via fluorescence microscopy during monolayer transfer to substrates. *Langmuir.* 14:2567–2572.

25. Majewski, J., R. Popovitz-Biro, W. G. Bouwman, K. Kjaer, J. Als-Nielsen, M. Lahav, and L. Leiserovitz. 1995. The structural properties of uncompressed crystalline monolayers of alcohols $CH_{2n+1}OH$ ($n = 13–31$) on water and their role as ice nucleators. *Chem. Eur. J.* 1:304–311.

26. Jensen, T. R., and K. Kjaer. 2001. Structural properties and interactions of thin films at the air-liquid interface explored by synchrotron X-ray scattering. *In* Novel Methods to Study Interfacial Monolayers, Vol. 11. D. Mobius and R. Miller, editors. Elsevier, Amsterdam, The Netherlands. 205–254.

27. Lee, K. Y. C., J. Majewski, T. L. Kuhl, P. B. Howes, K. Kjaer, M. M. Lipp, A. J. Waring, J. A. Zasadzinski, and G. S. Smith. 2001. Synchrotron x-ray study of lung surfactant-specific peptide SP-B in lipid monolayers. *Biophys. J.* 81:572–585.

28. Als-Nielsen, J., and K. Kjaer. 1989. X-ray reflectivity and diffraction studies of liquid surfaces and surfactant monolayers. *In* The Proceedings of the NATO Advanced Study Institute, Phase Transitions in Soft Condensed Matter. T. Riste and D. Shierrington, editors. Plenum, New York. 113.

29. Als-Nielsen, J., D. Jacquemain, K. Kjaer, F. Leveiller, M. Lahav, and L. Leiserowitz. 1994. Principles and applications of grazing incidence x-ray and neutron scattering from ordered molecular monolayers at the air-water interface. *Phys. Rep.* 246:252–313.

30. Ito, H., T. H. Morton, and V. Vodyanoy. 1989. Small odorant molecules affect steady-state properties of monolayers. *Thin Solid Films.* 180:1–13.

31. Phillips, M. C., and D. Chapman. 1968. Monolayer characteristics of saturated 1,2-diacyl phosphatidylcholines (lecithins) and phosphatidylethanolamines at air-water interface. *Biochim. Biophys. Acta.* 163:301–313.

32. Möhwald, H. 1990. Phospholipid and phospholipid-protein monolayers at the air/water interface. *Annu. Rev. Phys. Chem.* 41:441–476.

33. Knobler, C. M., and R. C. Desai. 1992. Phase-transitions in monolayers. *Annu. Rev. Phys. Chem.* 43:207–236.

34. Nag, K. K., and M. W. Keough. 1993. Epifluorescence microscopic studies of monolayers containing mixtures of dioleoylphosphatidylcholines and dipalmitoylphosphatidylcholines. *Biophys. J.* 65:1019–1026.

35. Gaines, G. L. 1966. *In* Interscience Monographs on Physical Chemistry: Insoluble Monolayers at Liquid-Gas Interfaces. I. Prigogine, editor. Interscience, New York. 281–300.

36. Seelig, A. 1987. Local-anesthetics and pressure—a comparison of dibucaine binding to lipid monolayers and bilayers. *Biochim. Biophys. Acta.* 899:196–204.

37. Diamant, H., T. A. Witten, C. Ege, A. Gopal, and K. Y. C. Lee. 2001. Topography and instability of monolayers near domain boundaries. *Phys. Rev. E.* 63:061602.

38. Hollars, C. W., and R. C. Dunn. 1998. Submicron structure in L-α dipalmitoylphosphatidycholine monolayers and bilayers probed with confocal, atomic force, and near-field microscopy. *Biophys. J.* 75:342–352.

39. Majewski, J., T. L. Kuhl, K. Kjaer, and G. S. Smith. 2001. Packing of ganglioside-phospholipid monolayers: an x-ray diffraction and reflectivity study. *Biophys. J.* 81:2707–2715.

40. Fang, J., and C. M. Knobler. 1995. Control of density in self-assembled organosilane monolayers by Langmuir-Blodgett deposition. *J. Phys. Chem.* 99:10425–10429.

41. McIntosh, T. J., and S. A. Simon. 1994. Long- and short-range interactions between phospholipid/ganglioside GM1 bilayers. *Biochemistry.* 33:10477–10486.

42. Guinier, A. 1968. X-ray Diffraction in Crystals, Imperfect Crystals, and Amorphous Bodies. W. H. Freeman & Company, San Francisco.

43. Kuhl, T. L., J. Majewski, P. B. Howes, K. Kjaer, A. von Nahmen, K. Y. C. Lee, B. Ocko, J. N. Israelachvili, and G. S. Smith. 1999. Packing stress relaxation in polymer-lipid monolayers at the air-water interface: an X-ray grazing-incidence diffraction and reflectivity study. *J. Am. Chem. Soc.* 121:7682–7688.

44. Luckham, P., J. Wood, S. Froggatt, and R. Swart. 1993. The surface properties of gangliosides. I. Monolayer properties. *J. Colloid Interface Sci.* 156:164–172.

45. Weng, K. C., J. L. Kanter, W. H. Robinson, and C. W. Frank. 2006. Fluid supported lipid bilayers containing monosialoganglioside GM1: a QCM-D and FRAP study. *Colloids Surf. B.* 50:76–84.

46. Heywang, C., G. Mathe, D. Hess, and E. Sackmann. 2001. Interaction of GM_1 glycolipid in phospholipid monolayers with wheat germ agglutinin: effect of phospholipid environment and subphase. *Chem. Phys. Lipids.* 113:41–53.

47. Maggio, B., F. A. Cumar, and R. Caputto. 1978. Interactions of gangliosides with phospholipids and glycoshingolipids in mixed monolayers. *Biochem. J.* 175:1113–1118.

48. Gericke, A., A. Kerth, and A. Blume. 1999. Infrared spectroscopic investigation of lipid and protein monolayers at the air/water interface. Bruker Application Note 51.

49. Lee, K. Y. C., A. Gopal, A. von Nahmen, J. A. Zasadzinski, J. Majewski, G. S. Smith, P. B. Howes, and K. Kjaer. 2002. Influence of palmitic acid and hexadecanol on the phase transition temperature and molecular packing of dipalmitoylphosphatidyl-choline monolayers at the air-water interface. *J. Chem. Phys.* 116:774–783.

50. Brocca, P., P. Berthault, and S. Sonnino. 1998. Conformation of the oligosaccharide chain of G_{M1} ganglioside in a carbohydrate-enriched surface. *Biophys. J.* 74:309–318.

51. Acquotti, D., and S. Sonnino. 2000. Use of nuclear magnetic resonance spectroscopy in evaluation of ganglioside structure, conformation, and dynamics. *Methods Enzymol.* 312:247–272.

52. Arnulphi, C., C. A. Martin, and G. D. Fidelio. 2003. Mixed lipid aggregates containing gangliosides impose different ^{2}H-NMR dynamical parameters on water environment depending on their lipid composition. *Mol. Membr. Biol.* 20:319–327.

53. Müller, E., A. Giehl, G. Schwarzmann, K. Sandhoff, and A. Blume. 1996. Oriented 1,2-dimyristoyl-*sn*-glycero-3-phosphorylcholine/ganglioside membranes: a Fourier transform infrared attenuated total reflection spectroscopic study. Band assignments: orientational, hydrational, and phase behavior; and effects of Ca^{2+} binding. *Biophys. J.* 71:1400–1421.

54. Takizawa, T., Y. Nakata, A. Takahashi, M. Hirai, S. Yabuki, and K. Hayashi. 1998. Differential scanning calorimetry and ^{1}H-NMR study of aqueous dispersions of the mixtures of dipalmitoylphosphatidilcholine and phosphatidylinositol-4,5-bis(phosphate). *Thermochim. Acta.* 308:101–107.

55. Bordi, F., C. Cametti, F. De Luca, T. Gili, D. Gaudino, and S. Sennato. 2003. Charged lipid monolayers at the air-solution interface: coupling to polyelectrolyes. *Colloids Surf. B.* 29:149–157.

56. Gurtovenko, A. A., M. Patra, M. Karttunen, and I. Vattulainen. 2004. Cationic DMPC:DMTAP Lipid Bilayers: Molecular Dynamics Study. *Biophys. J.* 86:3461–3472.

57. Levadny, V., and M. Yamazaki. 2005. Cationic DMPC:DMTAP lipid bilayers: local lateral polarization of phosphatidylcholine headgroups. *Langmuir.* 21:5677–5680.

58. Brezesinski, G., A. Dietrich, B. Struth, C. Böhm, W. G. Bouwman, K. Kjaer, and H. Möhwald. 1995. Influence of ether linkages on the structure of double-chain phospholipid monolayers. *Chem. Phys. Lipids.* 76:145–157.

59. Imura, T., H. Sakai, H. Yamauchi, K. Kozawa, S. Yokoyama, M. Matsumota, and M. Abe. 2000. Atomic force microscopic study on the surface properties of phospholipid monolayers containing ceramide 3. *Colloids Surf. B.* 19:81–87.

60. Massey, J. B. 2001. Interaction of ceramides with phosphatidylcholine, sphingomyelin and sphingomyelin/cholesterol bilayers. *Biochim. Biophys. Acta. Biomemistry.* 1510:167–184.

61. Baekmark, T. R., G. Elender, D. D. Lasic, and E. Sackmann. 1995. Conformational transitions of mixed monolayers of phospholipids and poly(ethylene oxide) lipopolymers and interaction forces with solid surfaces. *Langmuir.* 11:3975–3987.